Università degli Studi di Napoli "Federico II"

SCUOLA POLITECNICA E DELLE SCIENZE DI BASE

DIPARTIMENTO DI INGEGNERIA INDUSTRIALE

CORSO DI LAUREA IN INGEGNERIA AEROSPAZIALE

CLASSE DELLE LAUREE IN INGEGNERIA INDUSTRIALE (L-9)

Elaborato di laurea in Meccanica del Volo

Modelling of a 19-pax scaled airplane model and preliminary evaluation of its stability and control characteristics

Relatore:
Prof. Danilo Ciliberti

Candidato:
Valentina Nasti
Matr. N35003199

ANNO ACCADEMICO 2021 – 2022

Alla mia famiglia.
E a quella parte di me che ci ha sempre creduto.

Abstract

The purpose of this work is to perform an analysis of an aircraft, the PROSIB 19 pax.
The analysis is performed using VSPAero software, after the geometric modeling of the aircraft is done on OpenVSP. Vehicle Sketch Pad describes geometry using terms most familiar to designers, simplifying design. OpenVSP is a parametric aircraft geometry tool which allows the user to create a 3D model of an aircraft defined by engineering parameters. The program gives correct and reliable results if the simulation is carefully set up. In this case, the software has proved to be fast in analysis and very convenient, starting from the geometric design to the data analysis. The solver used is Vortex Lattice Method, which is a numerical method used in computational fluid dynamics, generally in the early stages of design. This models the leading surfaces by assimilating them to an infinitely thin sheet of discrete vortices. Of course, the model used in simulations must be carefully refined to obtain relevant results. The software certainly has limits for more complex models, however, it has been shown that it is a good solution for simple projects that require a first numerical analysis to be compared with real tests in the wind tunnel.

Sommario

Lo scopo di questo lavoro è quello di eseguire l''analisi di un velivolo, il PROSIB 19 pax. L'analisi viene eseguita utilizzando il software VSPAERO, dopo che la modellazione geometrica del velivolo è eseguita su OpenVSP. Vehicle Sketch Pad descrive la geometria utilizzando i termini più familiari ai progettisti, semplificando il design. OpenVSP è uno strumento parametrico di geometria dell'aeromobile che consente all'utente di creare un modello 3D di un aeromobile definito da parametri ingegneristici. Il programma fornisce risultati corretti e affidabili se la simulazione è impostata con attenzione. In questo caso, il software ha dimostrato di essere veloce nell'analisi e molto conveniente, a partire dal disegno geometrico all'analisi dei dati. Il solutore utilizzato è il Vortex Lattice Method, che è un metodo numerico utilizzato nella fluidodinamica computazionale, generalmente nelle prime fasi di progettazione. Quest'ultimo modella le superfici portanti assimilandole ad un foglio infinitamente sottile di vortici discreti. Naturalmente, il modello utilizzato nelle simulazioni deve essere accuratamente perfezionato per ottenere risultati pertinenti. Il software ha certamente dei limiti per modelli più complessi; tuttavia, è stato dimostrato che è una buona soluzione per progetti semplici che richiedono una prima analisi numerica da confrontare con prove reali in galleria del vento.

Table of contents

List of figures

List of tables

1. Introduction

1.1 Objectives

The purpose of the work is to fully represent the aerodynamic and stability analysis of the PROSIB 19-pax. The object of the thesis is to provide preliminary data on stability and control of an aircraft model to be tested in the wind tunnel. The thesis also aims to explicate the VLM numerical method, its basic theory and how this method is related to the software used. Also shown is the data collection, performed using VSPAERO and processed with Microsoft Excel. The latter contains the Lift, aerodynamic efficiency, Moment coefficient and drag polar curves for isolated wing, partial aircraft and complete aircraft, obtained from data processing on Excel. The effect of the fuselage is shown, and then also the effect of flaps at three different angles of deflection. Finally, aircraft stability considerations are also made using a table obtained by starting the analysis at a specific angle of attack.

1.2 Layout of the work

Chapter 2: This chapter discusses the theoretical foundations of the VLM method and its assumptions.

Chapter 3: This chapter deals with VSPAERO and OpenVSP, with an overview of their main functions.

Chapter 4: This chapter explains the process of geometric modeling and Refinement.
It also illustrates process of analyzing the aerodynamic coefficients as the Chordwise and Spanwise parameters W and U change, and how the choice of two specific values of these parameters is made to fix a grid on the wing.

Chapter 5: The fifth section of the thesis discusses the data collected through the program, their organization in graphs and tables, and comparisons between the various curves.

Chapter 6: Conclusions chapter.

2. Vortex Lattice Method

2.1 Theoretical Background

Computational aerodynamics succeeds in providing information on complex problems by solving the equations that control fluid dynamics.
Considering an inviscid, incompressible flow, potential flow provides sufficient results under a wide range of conditions. Laplace's equation is an exact representation of this flow.
Starting with irrotational flow, which is defined as a flow where the vorticity is zero at every point.

$$\xi = \nabla \times V = 0$$

In the case ϕ is a scalar function, we get

$$\nabla \times (\nabla \phi) = 0$$

Combining the two formulas, we get

$$\mathrm{V} = \nabla \phi$$

The equation previously written, states that for irrotational flow there is a scalar function ϕ such that the velocity is given by the gradient of ϕ. We will therefore consider ϕ as the velocity potential.
From the principle of conservation of mass for an incompressible flow, we obtain the following expression:

$$\nabla \cdot V = 0$$

With the definition of velocity potential φ, for an incompressible and irrotational flow, we can combine the two previous formulas and obtain:

$$\nabla \cdot (\nabla \phi) = 0$$

Or

$$\nabla^2 \phi = 0$$

The above equation is the **Laplace equation**, which is responsible for regulating irrotational and incompressible flow. So, a complicated flow model for an irrotational and incompressible flow can be synthesized by summing a series of elementary flows that are also irrotational and incompressible. The VLM is based on these line vortices.

Regarding the boundary conditions, the VLM goes to linearize and transfer by making a linear approximation between velocity and pressure.

After linearly approximating, for the cases where the linearized relationship of the pressure coefficients is valid, the thickness does not contribute to the first-order lift of the velocity disturbance.

Considering a symmetric airfoil, the camber effect can also be neglected; after applying this boundary condition to the Laplace equation, the problem can be solved by including the effect of angle of attack on a plane surface.

When considering the boundary condition of a wing, the above condition states that the normal flow through the thin solid surface of the wing is zero.

This means that the sum of the normal component of the velocity induced by the wing vortices from the wake is zero. A solution of the Laplace equation is the singularity of the point vortex: Γ is called the circulation force of the vortex. The latter has the same sign as vorticity, clockwise positive.

The concept of point vortex can be extended to a general filament of three-dimensional vortex.

The mathematical model that describes the flow induced by this filament is the **Biot-Savart** law. It states that the increase in velocity dV at a point P due to a segment of a vortex filament dl at a point q is

$$dV_p = \frac{\Gamma}{4\pi} \cdot \frac{\mathrm{dl} \times r_{pq}}{|r_{pq}|^3}$$

This value can be integrated over the entire length of the vortex filament to obtain the velocity induced at point P, obtaining

$$V_p = \frac{\Gamma}{4\pi} \cdot \int \frac{\mathrm{dl} \cdot r_{pq}}{|r_{pq}|^3}$$

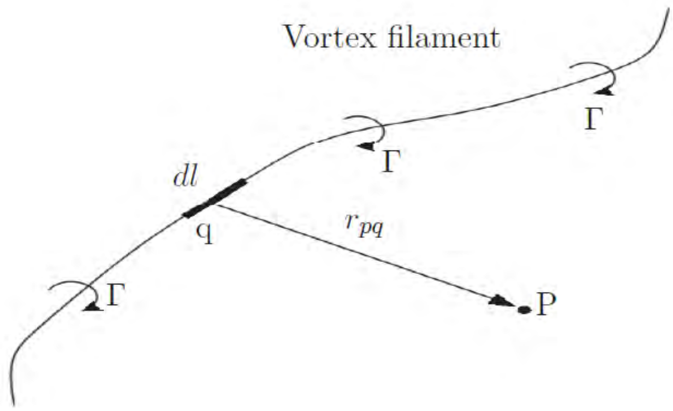

Figure 2.1 Three-dimensional vortex filament (Liu 2007).

It is also necessary to introduce the horseshoe vortex, a vortex in which the vortex line is assumed to be positioned in the x-y plane. It consists of four vortex filaments.

Two segments of the vortex are parallel to the direction of the free flow velocity and start from infinity, the other two segments are finite. In fact, we can consider the vortex to consist of only three parts, since the segment at the extremes can' be neglected because of the infinite distance. As mentioned above, the horseshoe vortex will represent a lifting surface.

The position of the vortex and the position of a control point are important to satisfy the boundary condition of the surface.

Thanks to the **Kutta-Joukowsky** theorem it is asserted that the lift is on bounded vortices.

The theorem asserts that a vortex of a given circulation Γ moving with free flow velocity Q∞ creates lift L.

As mentioned, the surface of the model is divided into a finite number of panels (transversely and longitudinally).

On each of these panels there is a horseshoe vortex, which has its own circulation and velocity. So, to obtain the total aerodynamic force, we need to add up the contribution of all the panels.

2.2 Practical implementation

The Vortex Lattice method is based on the following assumptions:

- The flow field is incompressible, inviscid and irrotational
- The lifting surfaces are thin. The influence of thickness on aerodynamic forces is neglected.
- The angle of attack and lateral slip angle are both small with a small angle approximation.

VLM has a limited region of application and accuracy, but despite this it is still widely used to study aerodynamic characteristics of aircraft. VLM (Vortex Lattice Method) is a numerical method used in computational fluid dynamics, mainly in the early stages of design.

This method goes on to model load-bearing surfaces (such as a wing for example) as an infinitely thin sheet of discrete vortices, going on to calculate Lift and Induced Resistance.

By simulating the flow field, one can' extract the pressure distribution, or as in the case of VLM the force distribution, around the simulated body.

From this, aerodynamic coefficients useful in the conceptual design phase can be estimated.

It should be emphasized that at this level it is not possible to evaluate viscous drag, but from lift it is possible to evaluate induced drag.

Since VLM is based on potential flow theory, its validity is limited to the linear aerodynamic region, thus purely related to low angles of attack, cruise range.

The effects of Mach number in subcritical flow can be considered by considering the Prandtl-Glauert correction, as anticipated in the previous section on the theoretical foundations of VLM. The VLM can be considered where the wing is modeled as an infinite number of horseshoe vortices.

So instead of a single horseshoe-shaped vortex for the wing, as in the Lifting Line Theory, the VLM uses a lattice of horseshoe-shaped vortices.

Key step is the approximation of the surface, for example, the wing can be approximated by its mean surface, then divided into flat quadrilateral panels.

So, we have a superimposition of a finite number of horseshoe vortices of different strengths Γ_n on the wing surface.

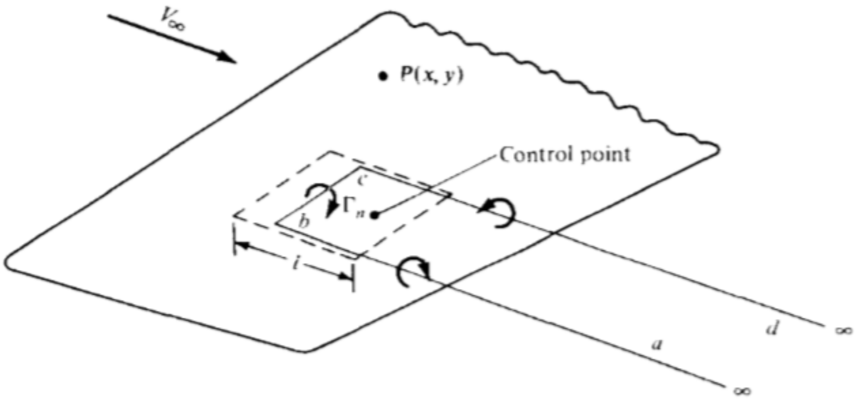

Figure 2.2 Representation of a single horseshoe vortex, which is a part of a vortex system.

The dashed lines define a panel on the wing shape, where l is the length of the panel in the direction of flow. A horseshoe vortex, abcd, of strength Γ_n, is positioned on the panel such that the segment bc (adherent part of a horseshoe vortex) is at distance $\frac{l}{4}$ from the edge of the panel. A control point is placed on the centerline of the panel at a distance of $\frac{3l}{4}$ from the front.

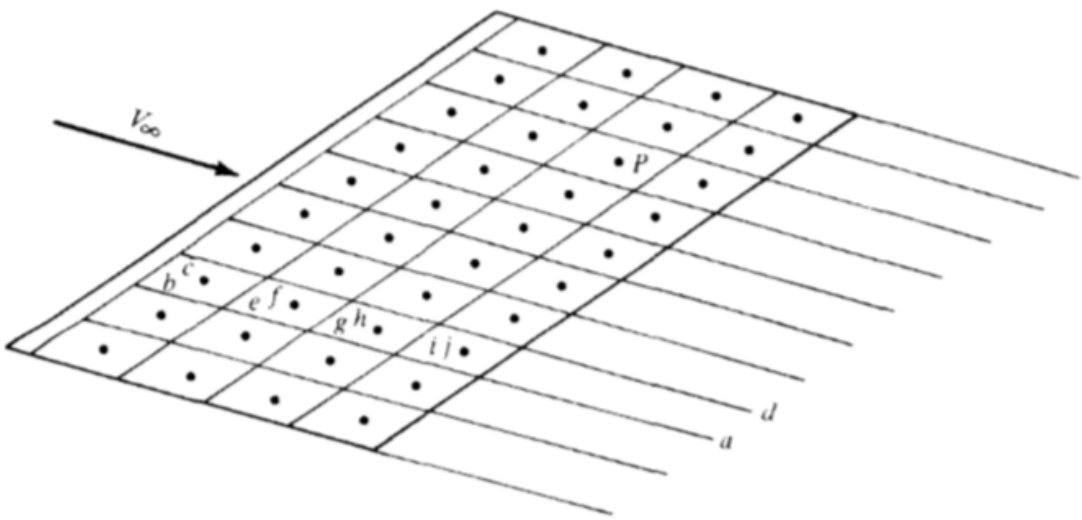

Figure 2.3 Representation of a Lattice of horseshoe vortex

The velocity induced at a point by a straight segment of a vortex filament is given by Biot-Savart's law. Unfortunately, the VLM fails near the leading edge of the wing and the tip, where the effect of thickness is significant.

Indeed, the problem is the inability of the method to calculate the local distribution of pressures; total and local forces are predicted at an acceptable level. An important assumption for further analysis of vortex-induced velocities at the control point is that the wake is assumed flat and lying in the plane of the wing at z=0. The number of vortices used varies with the resolution of the required pressure distribution and the accuracy of the calculated aerodynamic coefficients.

It is here remarked that that the VSPAERO solver is not based on the classical VLM in which the horseshoe vortices are distributed along the wing but is characterized by a ring of vortices and only the trailing vortices extend to infinity.

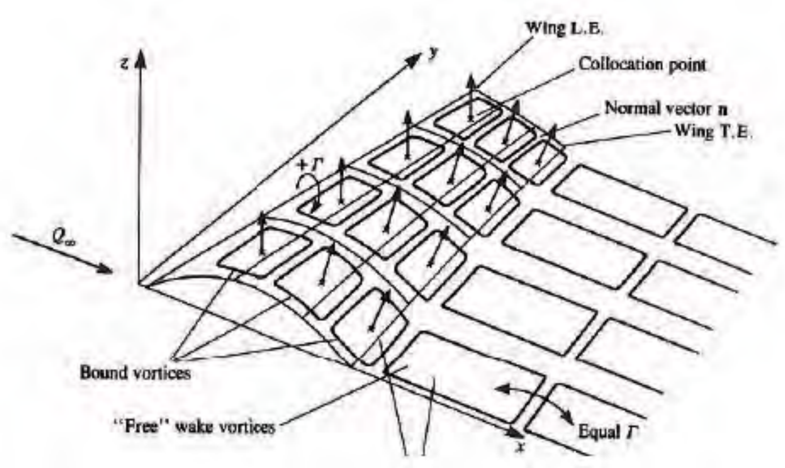

Figure 2.4 Representation of a Lattice of ring vortices

3. Geometric modeller

3.1 OpenVSP

OpenVSP is short for Open Vehicle Sketchpad. It is an open source parametric program aircraft geometry, originally developed by NASA. OpenVSP provides the user with the ability to create three-dimensional models of aircraft and perform engineering and aerodynamic analysis on those models (OpenVSP). The open-source code for OpenVSP was developed by Dave Kinney at NASA Ames. The software allows the user to create a 3D model of an aircraft defined by common engineering parameters. This model can be processed in formats suitable for engineering analysis. At the next link, you can access the OpenVSP Web site:

http://openvsp.org .After startup, OpenVSP displays a working window and a "Geometry Browser," which lists all the individual components of the user's model.

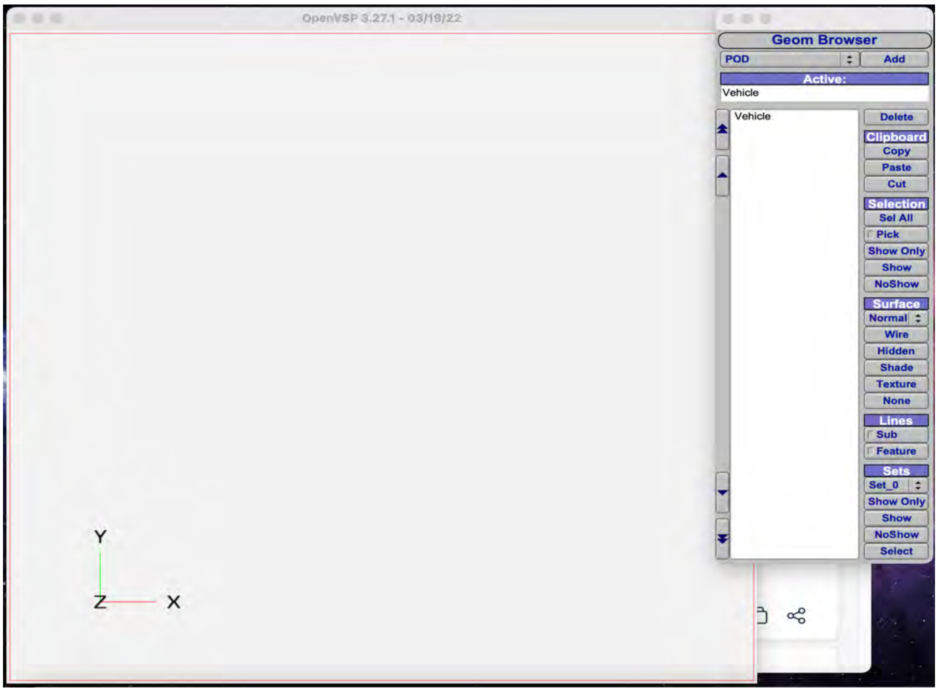

Figure 3.1 OpenVSP initial panel

When a component is selected, the component geometry window opens, which is used to change the parameters of the selected component. OpenVSP provides multiple geometries common to aircraft modeling that can be modified and assembled into an aircraft model, e.g., wing, pod, fuselage, propeller.

Figure 3.2 Possible geometries to select

Important is the setting of the U and W parameters of Spanwise and Chordwise, in the main panels. These parameters can be felt both for the total component and in the subsections (SECT in the geometry panel). This step will be very useful in the refinement we go on to do later. As we will see in the specific discussion of the geometry of the aircraft we are analyzing, each added geometric component (such as the wing), can be particularized in detail.

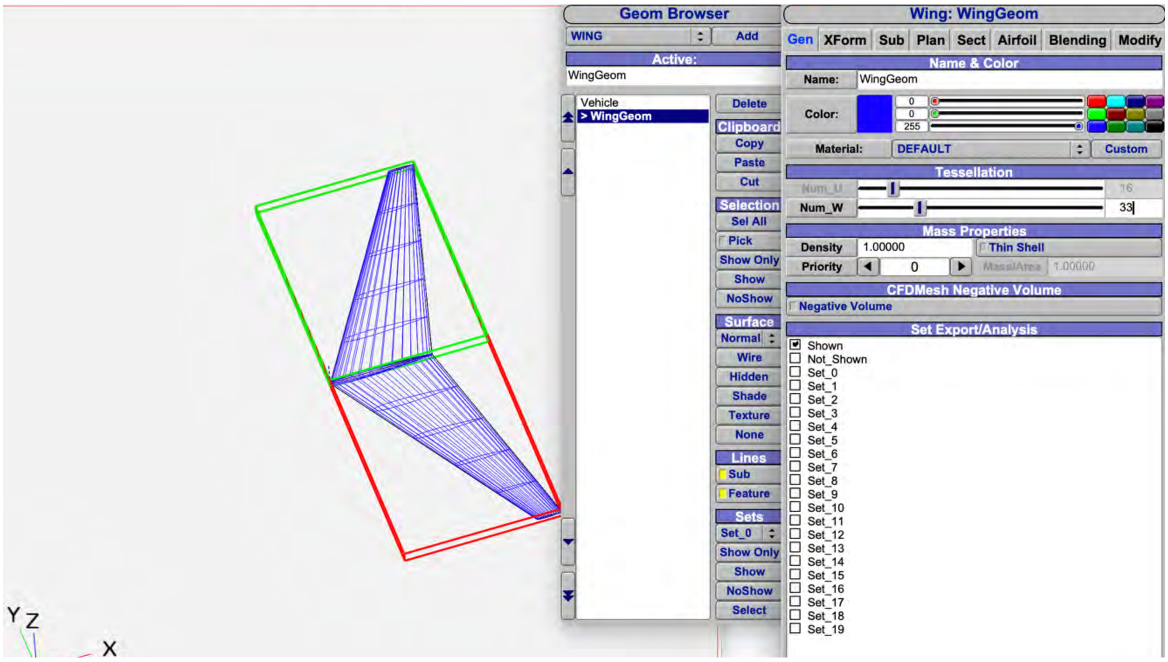

Figure 3.3 Panel for wing geometry and setting of U and W

3.2 VSPAERO

VSPAERO is a part of OpenVSP, was released in 2015. It is a thin-surface code for subsonic and supersonic inviscid aerodynamics.

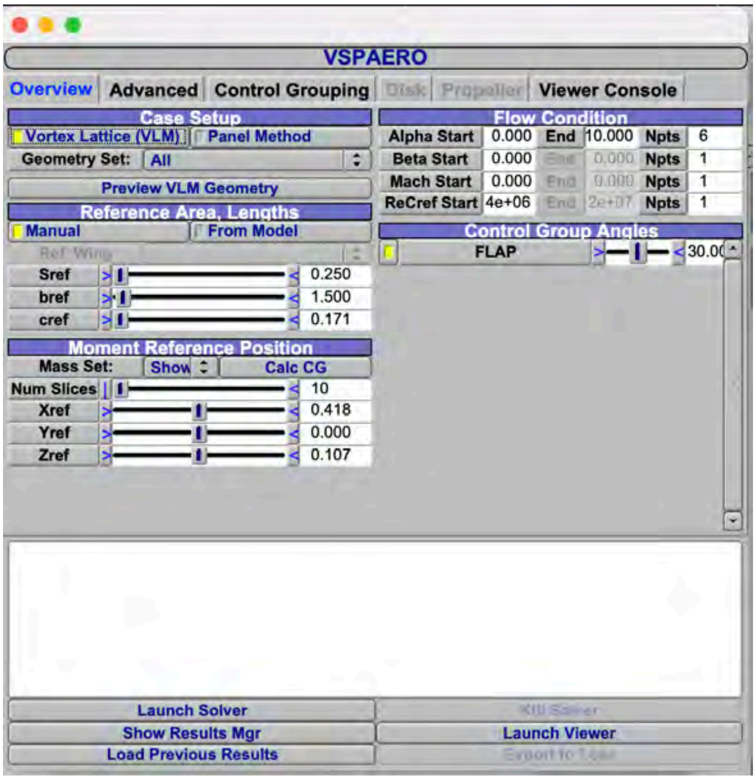

Figure 3.4 VSPAERO interface

VSPAERO includes a simple actuator disk model to represent propulsion-aircraft interaction and the ability to compute common stability derivatives. The software allows the definition of groups of control surfaces in the VSPAERO configuration file, facilitated by the Control Grouping tab of the VSPAERO GUI. The central "Available Control Surfaces" browser lists all rectangular surfaces and control subsurfaces that can be added to a control surface group. A control surface can be added to more than one group: Surface gains can be adjusted to allow mixing of control surfaces within a group. In geometry, a subsurface can also be added in the wing group. The one in question is a linear solver, so VSPAERO does not model stall or separation characteristics. It contains integrated actuator disks that can be accurately described for simple, rapid aero-propulsive analysis. It has a Viewer application that displays wakes and DeltaCp gradient (pressure coefficient change). The degenerate geometry file is required if you run VSPAERO's vortex lattice solver. Degenerate geometry files are

representations of three-dimensional models in progressively simple frames. A three-dimensional model is represented in its entirety, followed by a plane representation, followed by a stick representation.
VSPAERO analyzes the DegenGeom output file from VSP. An input file with operating conditions must be defined to start the analysis. The drag output provided contains only information about the induced part. Using components in the DegenGeom build file that do not affect lift will cause excessive operating time with no valuable return, such as the nacelle and fuselage. Therefore, when using VSPAero, the main components that control the output values are the lift surfaces such as the wing and horizontal stabilizer. While the other components will have a small effect on the aerodynamic drag of the vehicle, the induced drag that VSPAero determines is primarily based on the lift coefficient.
Now that our model has an associated DegenGeom file, we can begin writing our setup file. VSPAERO will recognize this file with the modelname DegenGeom.vspaero if we run the vortex lattice method. VSPAERO will write several files containing important information for model analysis.

- The "lod" file contains span load information (e.g., cCl section is given for each lifting component);
- The "adb" file contains information for VSPAERO;
- The "history" file contains the total integrated forces and moments;

The files appear in the OpenVSP folder containing both the execution files and the geometric model.

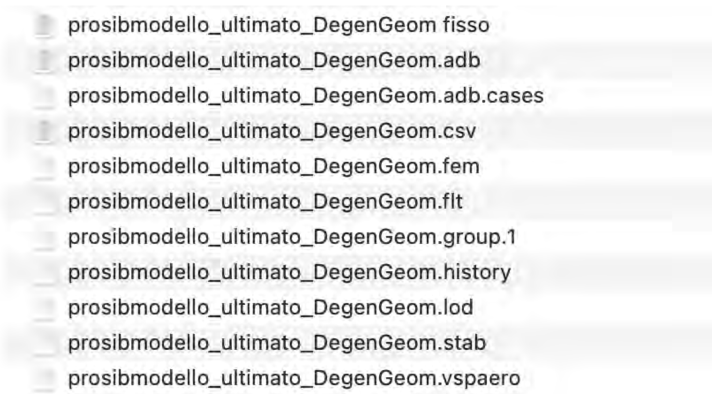

Figure 3.5 VSPAERO files folder

Files can be opened with software such as Notepad or Excel.

4. Geometric modeling and refinement

4.1 Wing Geometry introduction

In this paragraph, the first section of the chapter devoted to the aircraft geometry modeled with OpenVSP, we briefly describe the basic wing geometry, before describing in the following paragraphs the refinement by the choice of the W and U parameters. Therefore, it is a purely introductory chapter to make the subsequent paragraphs easier to understand.
The wing of our aircraft is designed as follows:

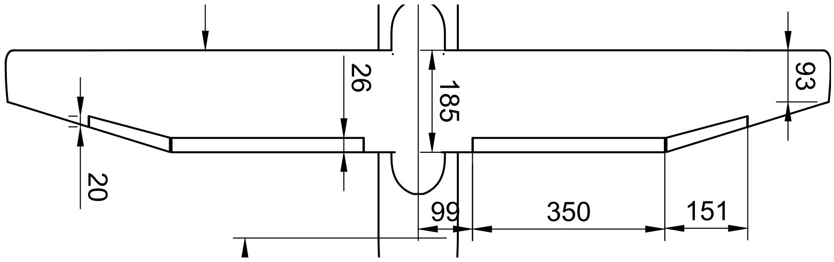

Figure 4.1 Wing Geometry

As anticipated, you are going to enter the dimensions (in mm scale) in the dedicated wing geometry panel (For now, the considerations of U and W are ignored).

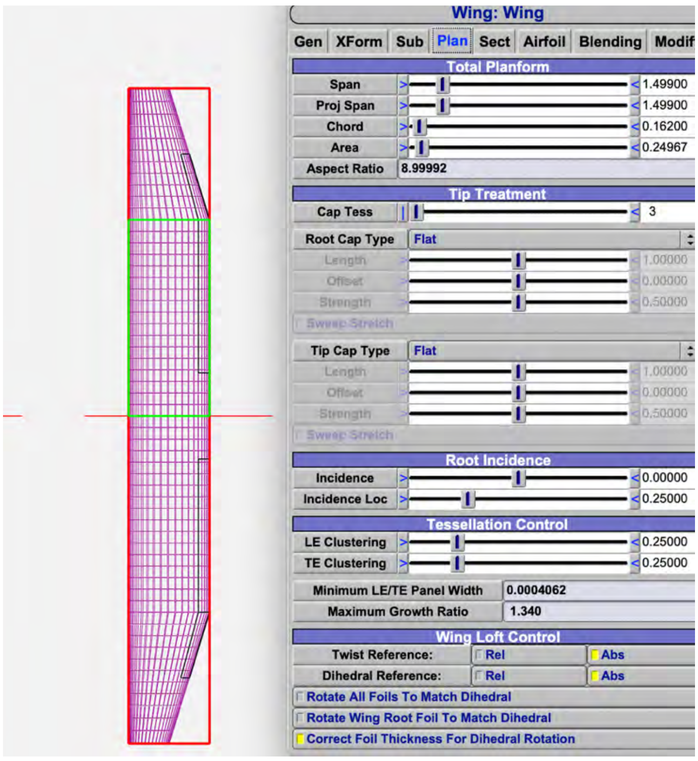

Figure 4.2 Main parameters of the wing

The wing has been divided into two sections:

Figure 4.3 Wing section panel

Each section, placed with respect to the semi-open consistent with the starting quotes, is characterized by an airfoil depending on if it is root, kink or tip. All quotes will be shown more fully in the general geometry section.

For our aircraft wing, we have NACA 23018 for root and kink, and NACA 23015 for tip.

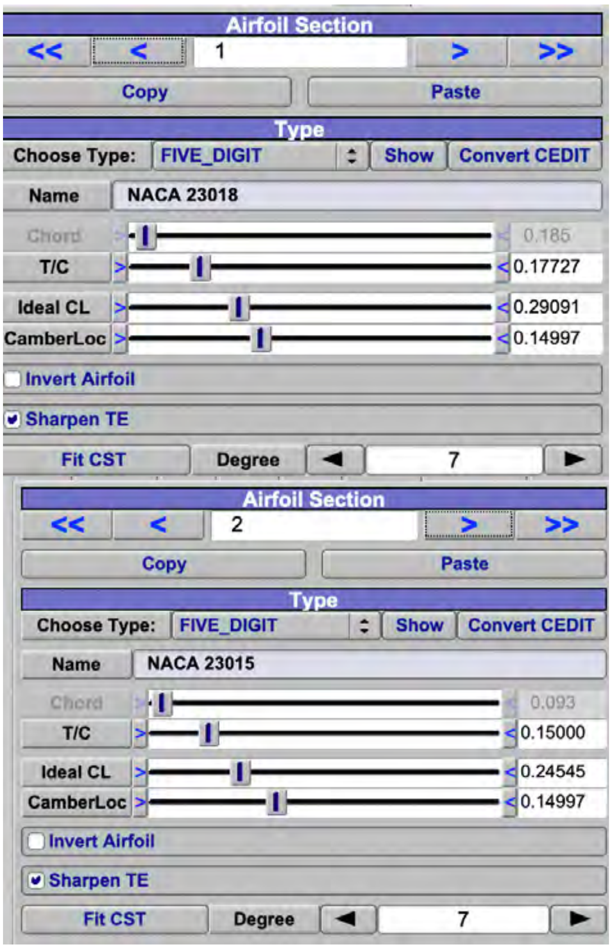

Figure 4.4 Wing Airfoil selection panel

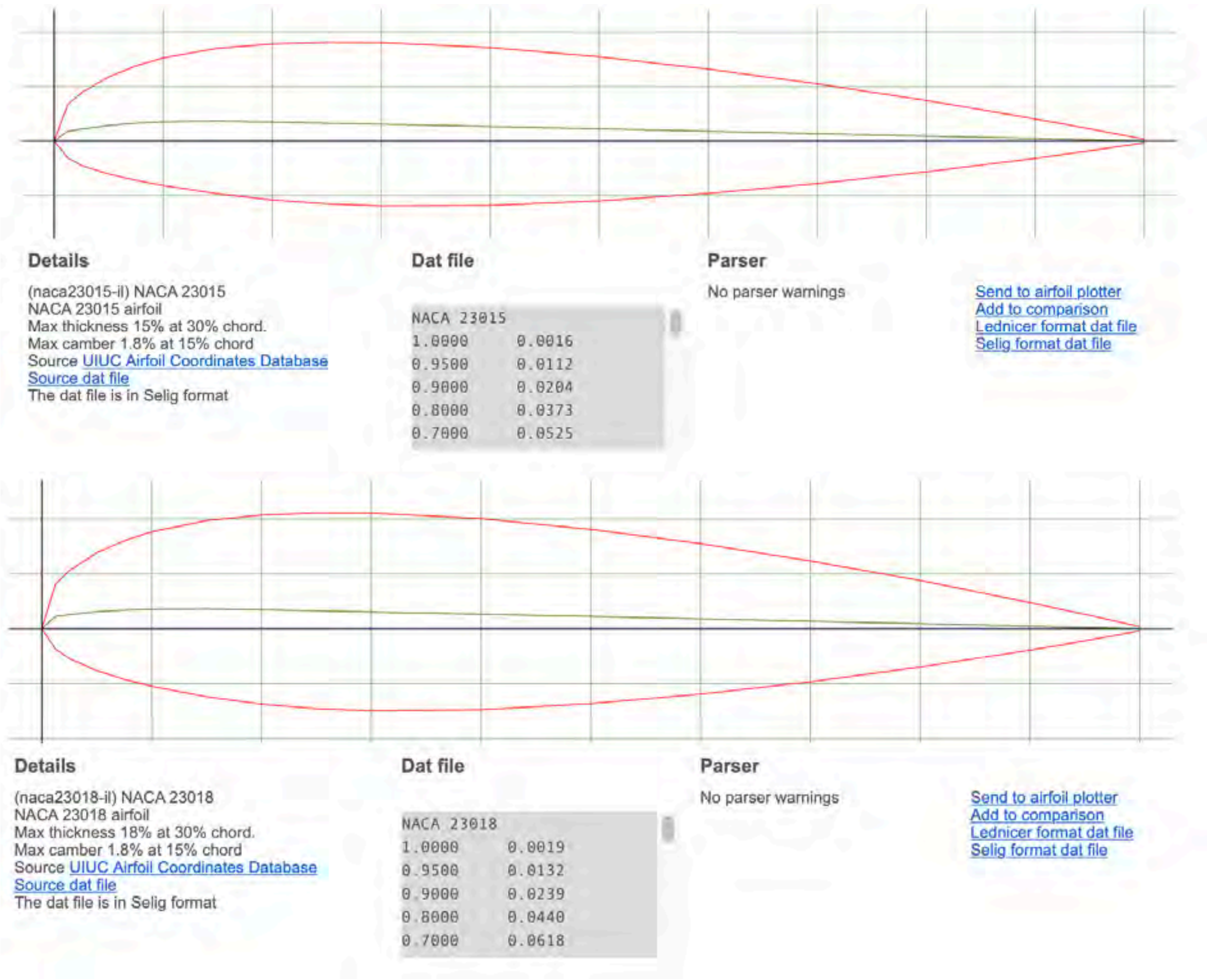

Figure 4.5 Airfoil images from http://airfoiltools.com

4.2 Wing Chordwise Refinement

Having briefly introduced the wing geometry of our aircraft, it is possible to proceed to the choice of the most suitable U and W values for fixing a wing grid and to proceed accordingly with the geometry of the aircraft. The first step is precisely Chordwise refinement by varying the W parameter. The model can be refined by changing the Num_W parameter in the Gen tab of the Wing Geometry window. The number of spanwise slices Num_U is kept on the default setting of 16.

We then vary the values of W 5 times, for 5, 13, 41, 69, 101, at a single angle of attack equal to α =0. Starting with a certain number of chordwise slices, the results for CL and the other coefficients change little if W is increased further. CL, CD and CM turn out to be relatively constant as Num_W changes.

Moreover, increasing or decreasing this number has negligible influence on the solution time.

For a certain value of W, expected asymptotic behavior occurs. The tables containing the variations and associated graphs are shown.

W	CL
5	0,06
13	0,09
41	0,09
69	0,09
101	0,10

W	Cdtot
5	0,00809
13	0,00827
41	0,00831
69	0,00831
101	0,00831

W	CMy
5	-0,022
13	-0,018
41	-0,020
69	-0,021
101	-0,021

Table 4.1- Tables of trends of the coefficients as W changes

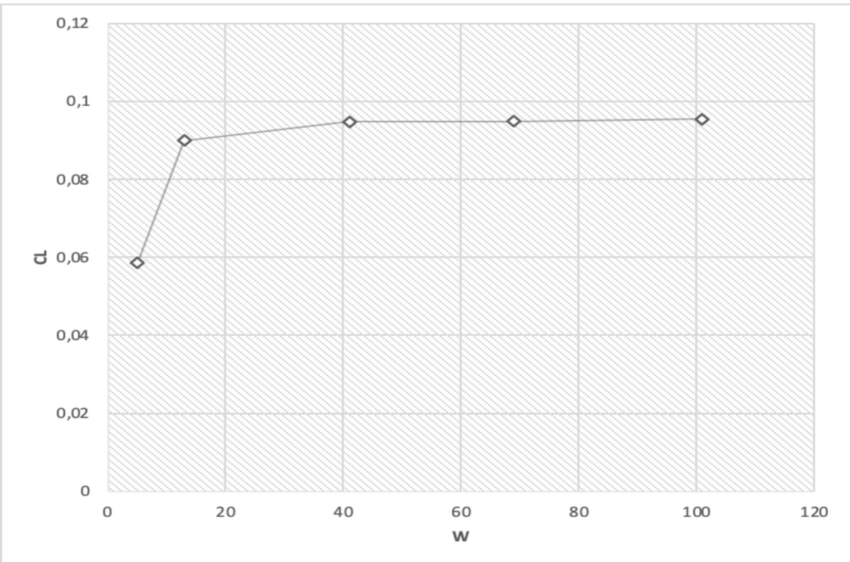

Figure 4.6 CL-W

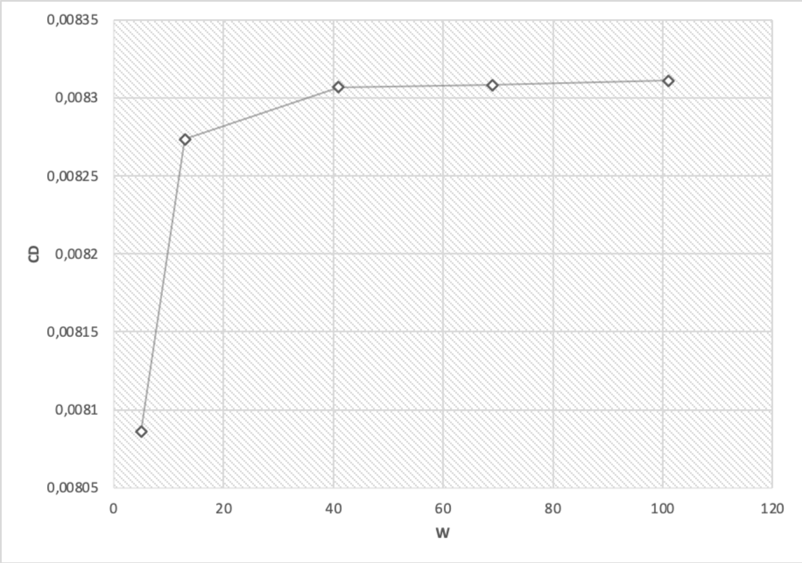

Figure 4.7 CD-W

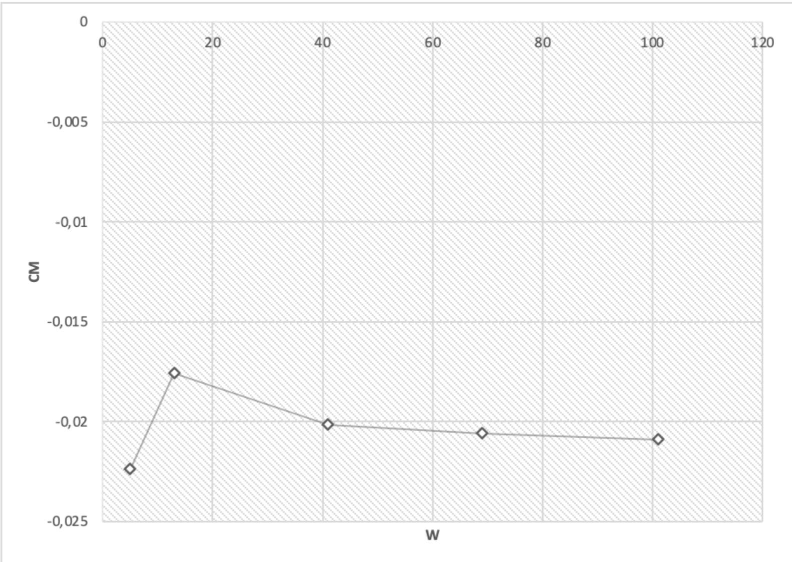

Figure 4.8 CM-W

Therefore, it can be concluded that the default number of Num_W (= 41) will be sufficient for the following experiments.

We then set W to 41, so that we can continue with the analyses to figure out the optimal value of U to choose (in the next section).

4.3 Wing Spanwise Refinement

After refinement in the longitudinal direction has been carried out, refinement in the transverse direction is also studied. This can be done by adjusting the Num_U parameter in the Sect tab of the Wing Geometry window.

By performing spanwise refinement, the expected asymptotic behavior is strongly visible by observing the Oswald efficiency factor. Increasing the number of spanwise panels clearly has a great influence on the simulation results.

The trends of the coefficients as U varies must be analyzed, this time keeping W fixed at the previously determined value, we vary U with W=41.

After showing these trends, we go, as before, to observe for a single angle of attack (in this case α=4), the trend of the coefficients as U changes. Four values of U are chosen: 10,30,50,70. The half-wing consists of two panels, visible in the SECT. This implies that the U will have to be distributed in their entirety, between the two panels of the half-wing (proportionally, of course). The two panels are quite similar to each other, it could choose a number of divisions proportional to the length of the panel.

With a proportion you get:

U	U_inner	U_outer
10	6	4
30	18	12
50	30	20
70	42	28

Table 4.2- Division of U over the two panels

U	CL
10	0,44
30	0,43
50	0,43
70	0,43

U	CDtot
10	0,0158
30	0,0158
50	0,0157
70	0,0157

U	CMy
10	-0,031
30	-0,030
50	-0,030
70	-0,030

Table 4.3- Tables of trends of the coefficients as U changes with fixed W=41

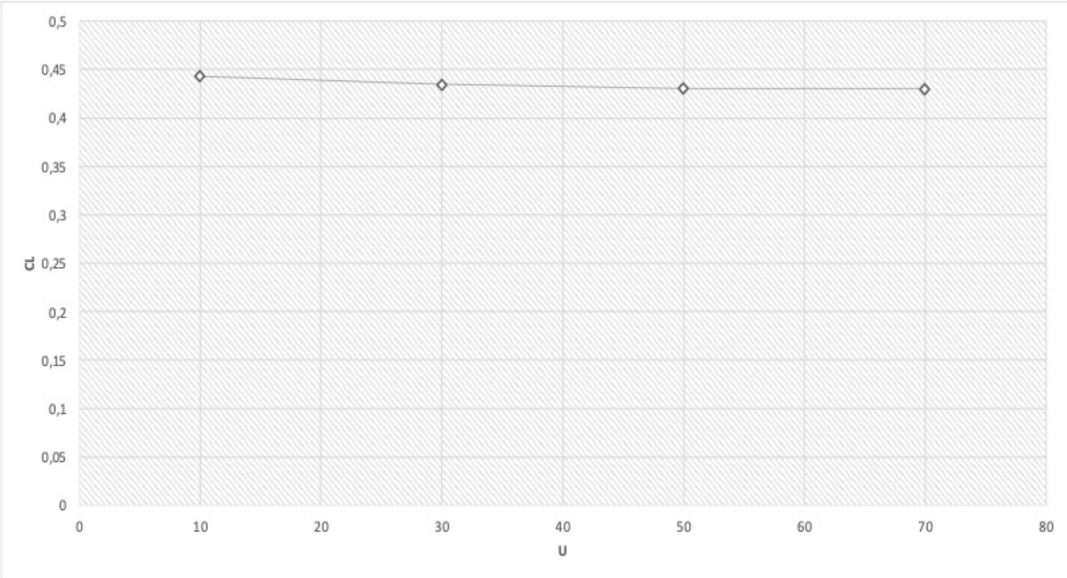

Figure 4.9 CL-U

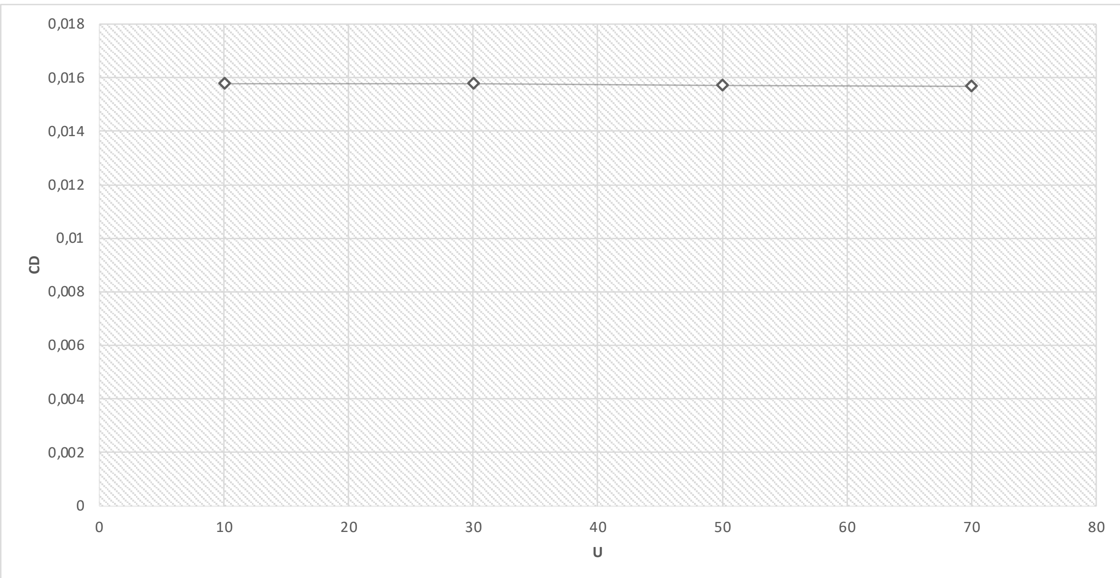

Figure 4.10 CD-U

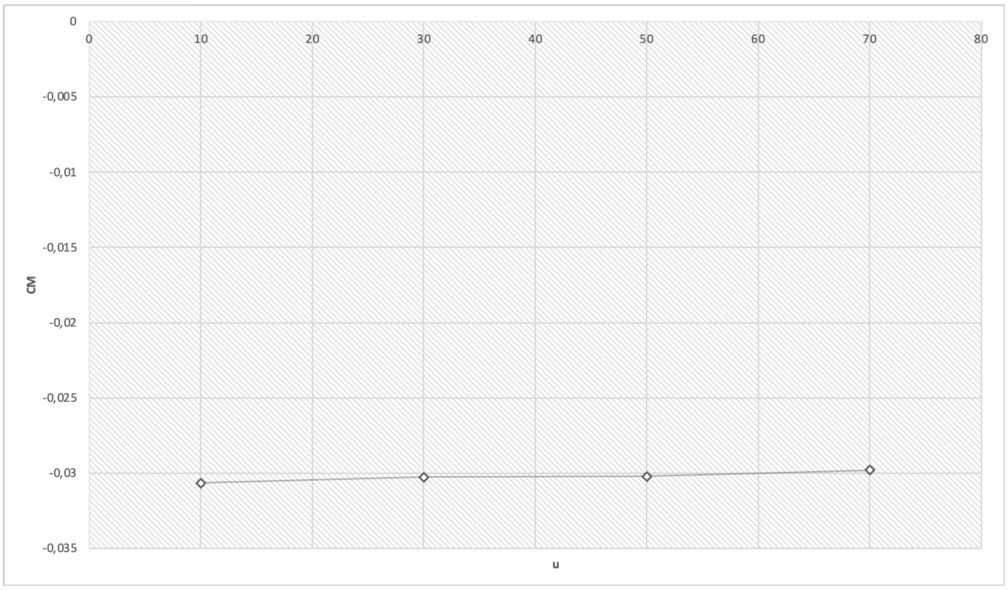

Figure 4.11 CM-U

As with W above, by looking at tables and graphs it is possible to show an optimal value of U, from which values then tend to be constant; thus, there is asymptoticity for U=30.

The wing grid therefore can be fixed for W=41 and U=30, (in the wing to be divided proportionally into the two sections, dividing it into 18 and 12). The same grid will be adopted for the Horizontal Tail.

4.4 Aircraft Geometry

4.4.1 Introduction

In the previous paragraphs we defined the wing, how to fix its grid and its geometric characteristics.

We now provide a description of the other elements of the scaled aircraft model, and then conclude in the next chapter with the most important aerodynamic analyses.

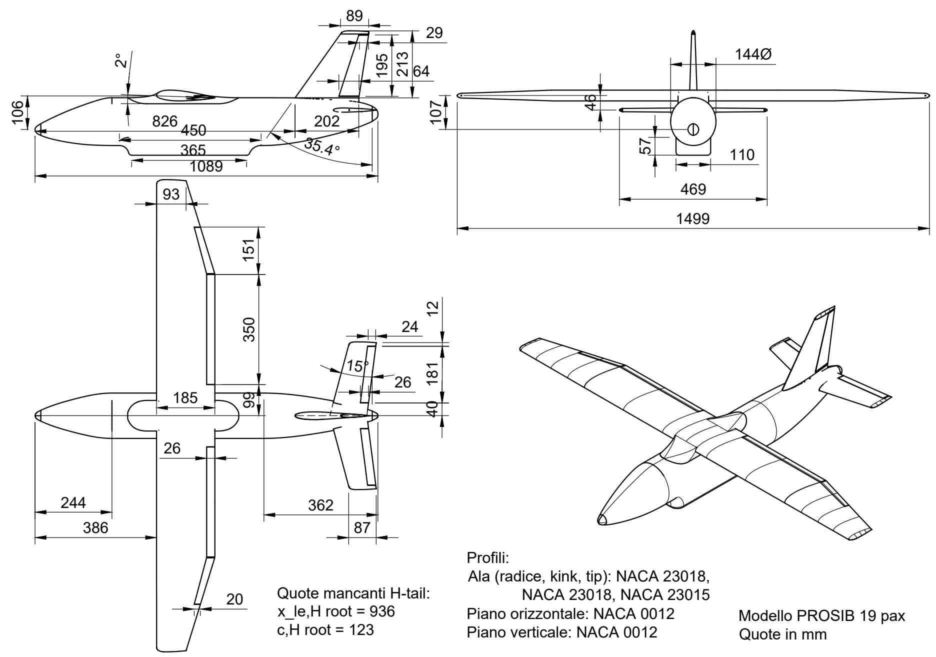

Figure 4.12 Aircraft Geometry

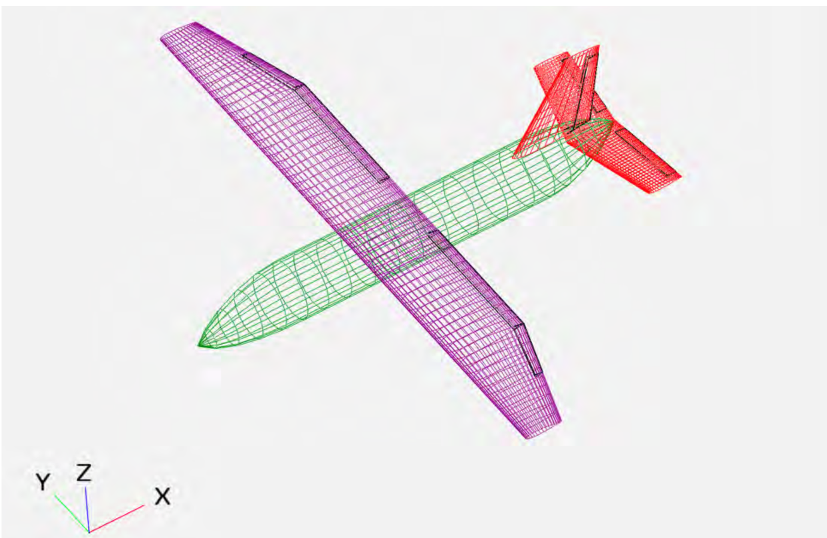

Figure 4.13 Aircraft OpenVSP Model

4.4.2 *Fuselage*

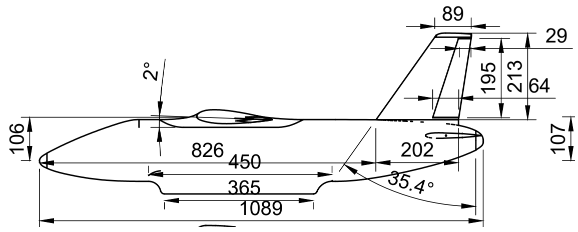

Figure 4.14 Fuselage Geometry

As with any geometric component, the fuselage also has a geometric modeling window. As with the wing you start modeling the component by entering the main dimensions in the Design panel.

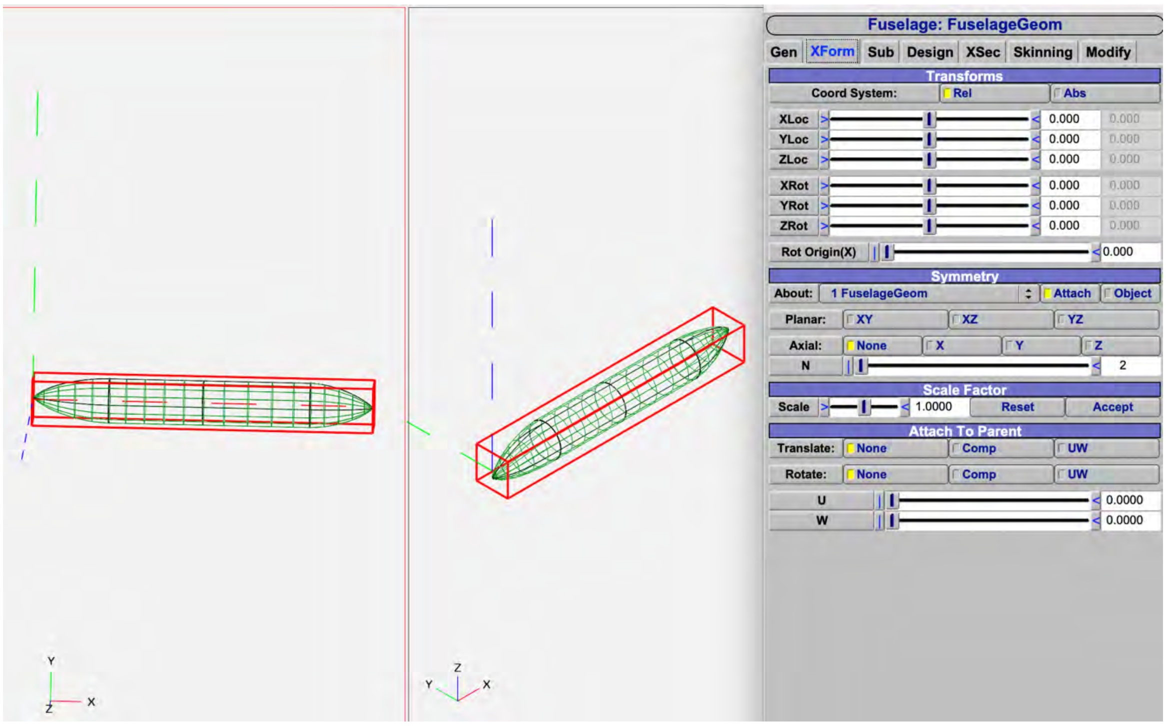

Figure 4.15 Fuselage design panel

Next you proceed to model section by section of the fuselage.

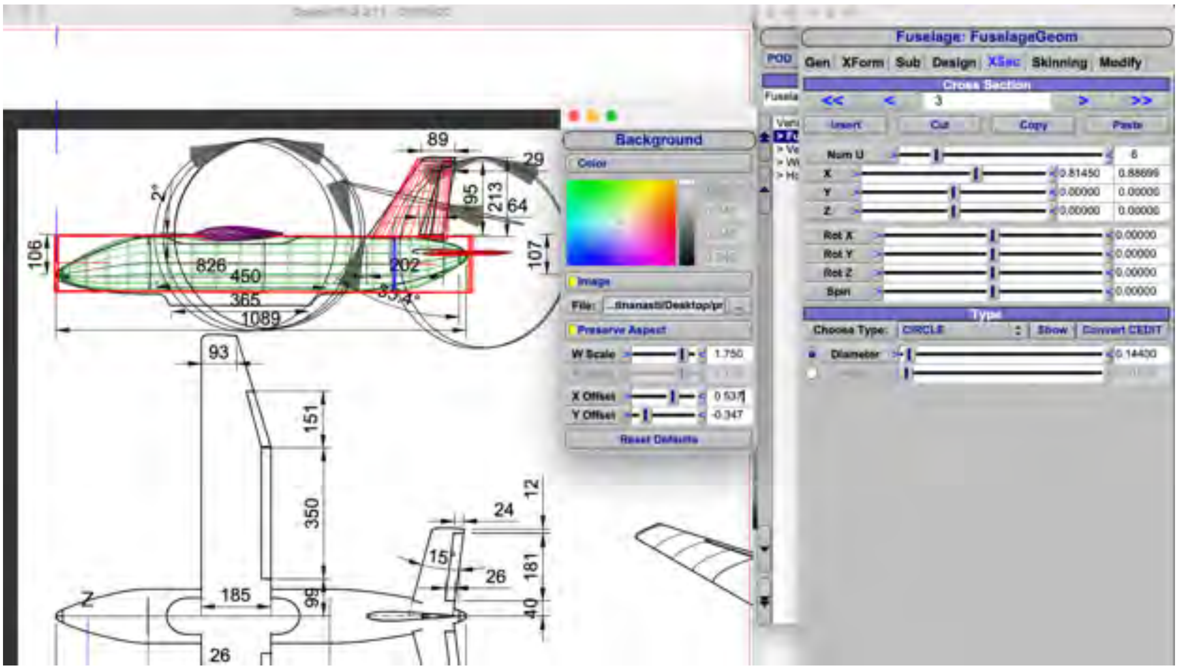

Figure 4.16 Refinement of fuselage curvature

Thanks to OpenVSP's feature of being able to place the design image behind the design window and being able to set the VSP model placement on it by 'similarity', it was possible to recreate the curvature of the fuselage, section by section by changing the parameter Z.

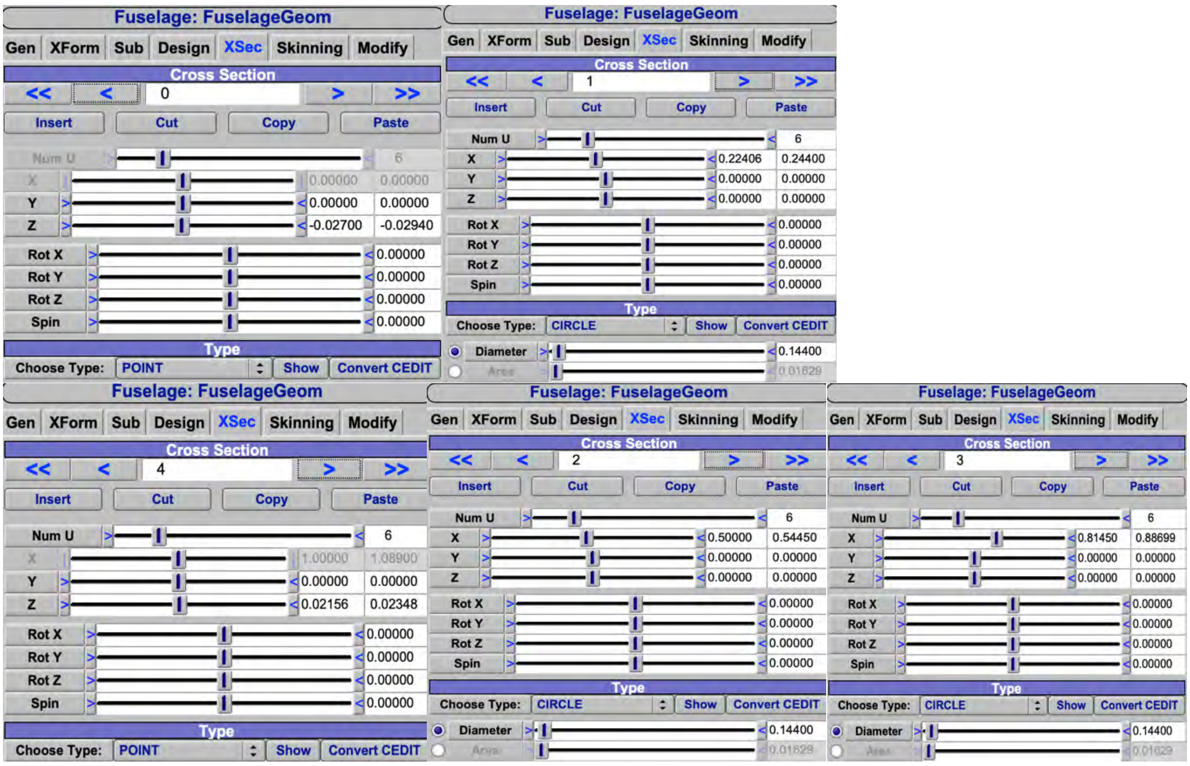

Figure 4.17 Design panel fuselage sections

4.4.3 Horizontal Tail

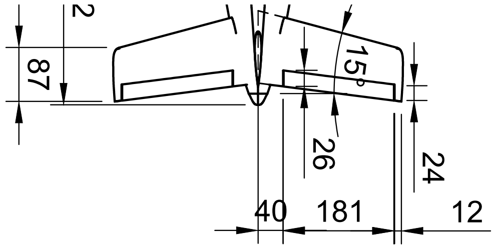

Figure 4.18 Horizontal Tail Geometry

Like the other components, the Horizontal Tail can also be modeled geometrically. Similar to the wing, the basic geometric parameters should be entered in the design window.

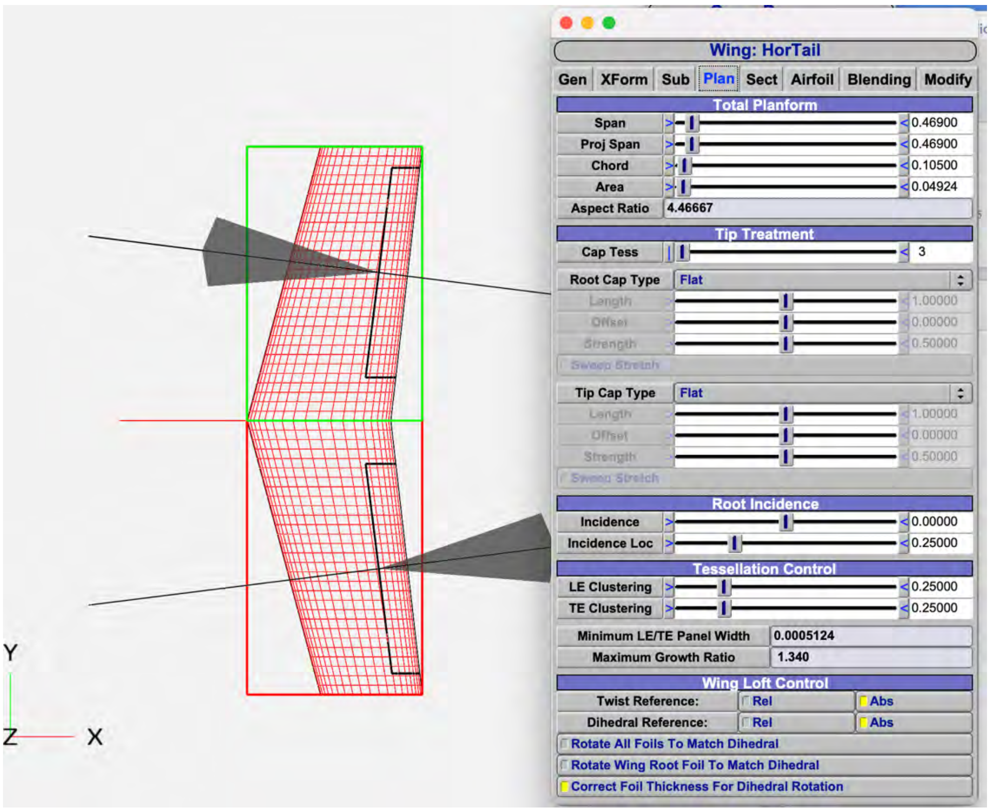

Figure 4.19 Horizontal Tail design panel

As with the wing, the airfoil assigned by the design is entered here.

Figure 4.20 Wing Airfoil selection panel

For the horizontal tail plane, the profile chosen is NACA 0012.

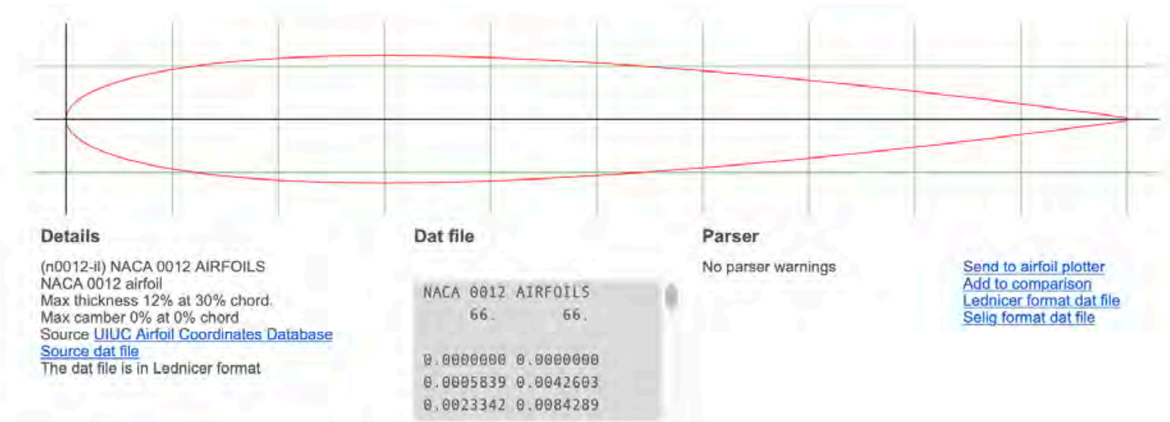

Figure 4.21 Airfoil image from http://airfoiltools.com

The same grid fixed for the wing, was also carried over for the horizontal tail. In the case of the horizontal tail, the grid for U is single, and not divided into the two sections as is the case for the wing.

4.4.4 Vertical Tail

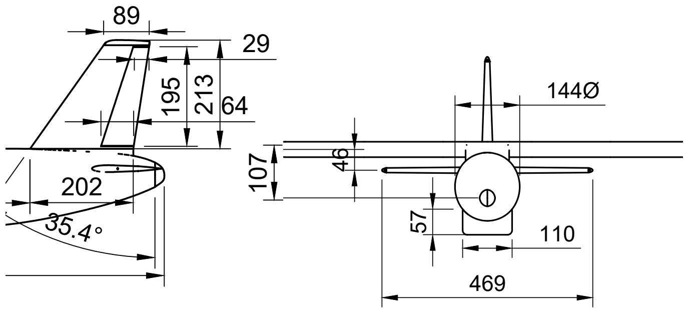

Figure 4.22 Vertical Tail Geometry

The tail plane is the last component to be modeled in our aircraft. We proceed as in the previous cases.

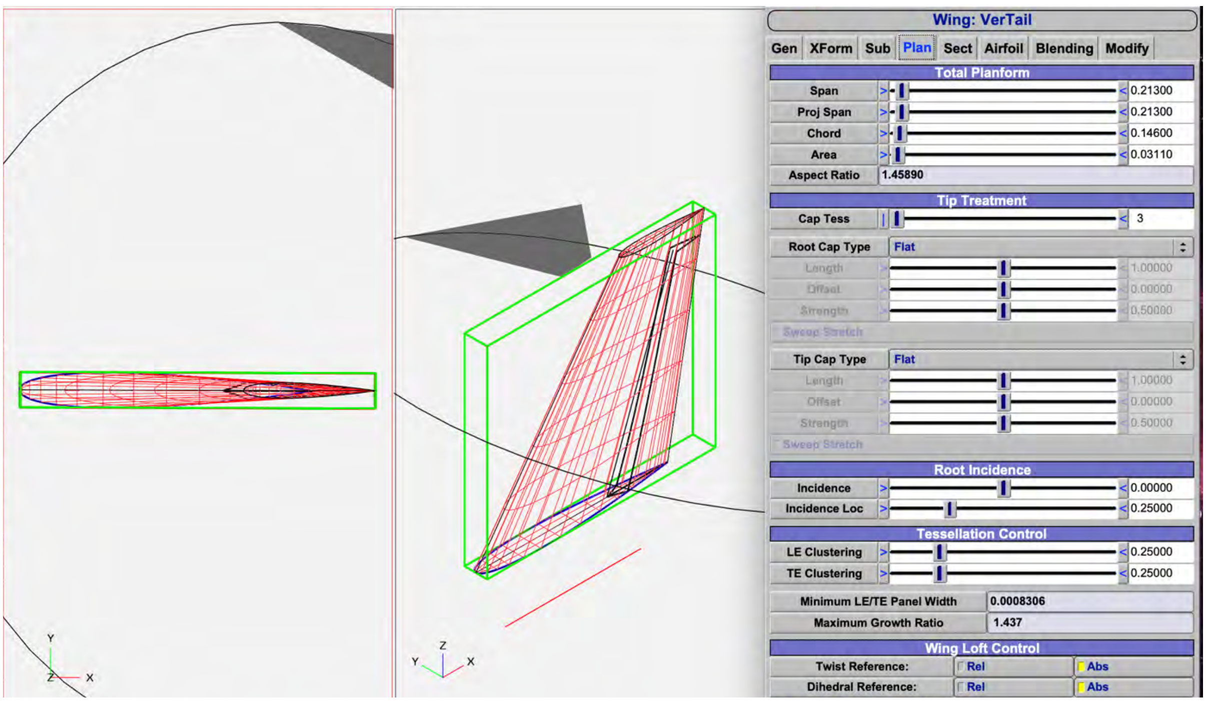

Figure 4.23 Vertical Tail design panel

As with the horizontal tail plane, the airfoil chosen is NACA 0012 already shown in the previous chapter.

4.4.5 Control Surfaces

The central “Available Control Surfaces” browser lists all control sub-surfaces that can be added to a group. To create a surface group, click the "Add" button under the "User Groups" browser. A control surface can be added to more than one group. When you select a control group, each control surface in the group appears under the "Deflection Gains per Surface" divider, where you can adjust the gains to allow mixing of control surfaces within a group.

Through the control group you can model the flaps. In the geometry, a subsurface can be added in the wing group. First you need to specify the type of sub-surface, and you can choose between line, rectangle, ellipse and control surface. Once the type is chosen, the boundary of the subsurface must be defined. Control surfaces have been entered for wing and tail planes. The effects of flap deflection will be shown in the next chapter.

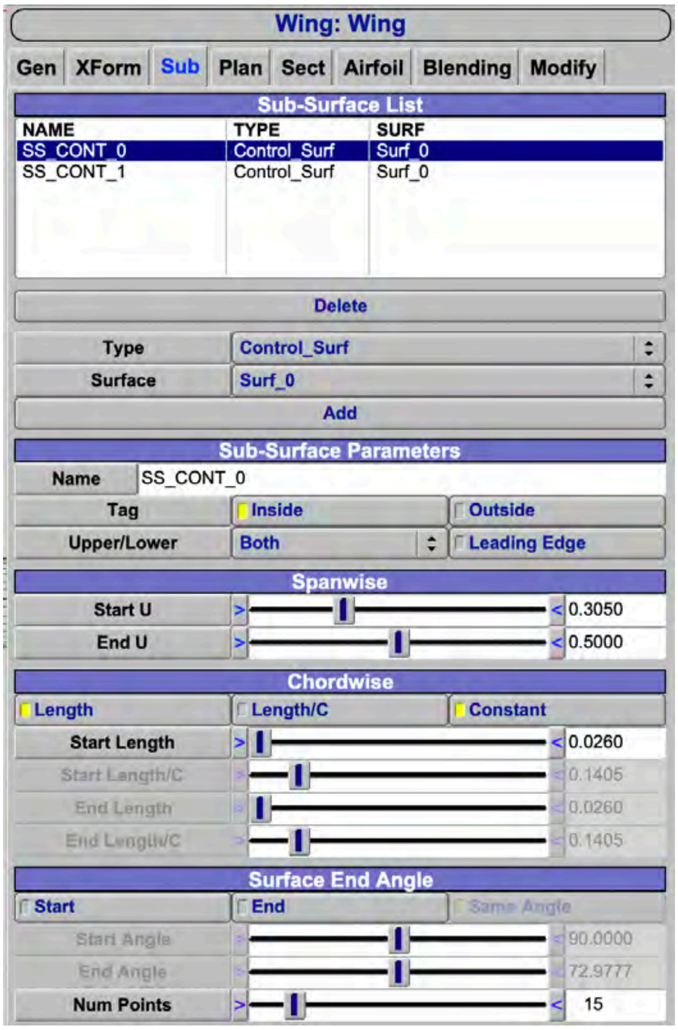

Figure 4.24 Wing Sub-Surface List

5. Results and discussion

5.1 Wing

Most of the paragraphs in this concluding chapter aim to show, now defined the geometry of the aircraft, the contributions of the individual components at the aerodynamic level. It starts precisely with the contributions related to the isolated wing. All calculations that will follow were performed, with the wing geometry fixed, thus with the grid set at W=41 and U=30.
The analysis on VSPAERO is performed working on 6 different angles of attack from 0 to 10.

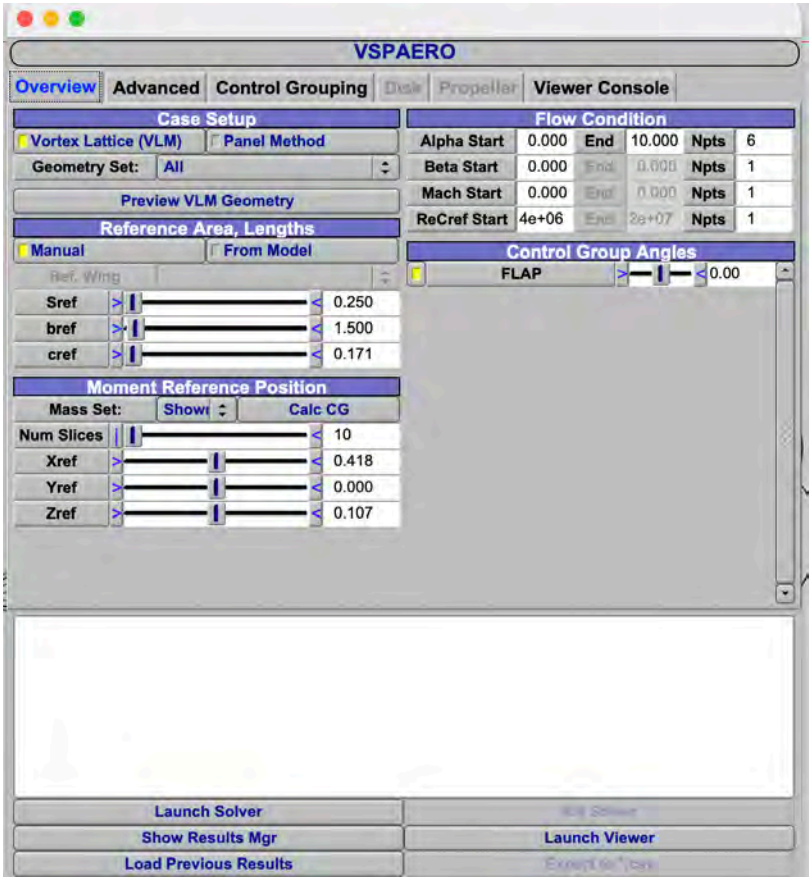

Figure 5.1 VSPAERO analysis panel

Through the panel showed in *Figure 5.1*, by selecting 'SET 0' (the set in which we entered only the wing), it is possible to start the analysis, with the parameter setting just as in the figure. In addition, we also need to tick 'X-Y Symmetry' in the 'Advanced' settings section. So, we obtain *Table 5.1*.

AoA	CL	CDtot	CL
0	0,09	0,00827	0,09
2	0,26	0,01075	0,26
4	0,43	0,01563	0,43
6	0,60	0,02287	0,60
8	0,77	0,03246	0,77
10	0,94	0,04434	0,94

AoA	CMy	AoA	CL/CD
0	-0,020	0	11,24
2	-0,026	2	24,34
4	-0,030	4	27,54
6	-0,033	6	26,21
8	-0,033	8	23,69
10	-0,032	10	21,15

Table 5.1- Wing tables of coefficient (angles in* deg*)

5.2 Wing and Horizontal Tail

By changing the SET of components in the analysis panel on VSPAERO, you can then proceed to compare wing and horizontal tailplane together.

AoA	CL	AoA	CL/CD
0	0,09	0	8,76
2	0,28	2	21,58
4	0,47	4	24,98
6	0,65	6	23,85
8	0,84	8	21,51
10	1,03	10	19,15

AoA	CMy	CDtot	CL
0	0,00	0,010	0,09
2	-0,07	0,013	0,28
4	-0,14	0,019	0,47
6	-0,20	0,027	0,65
8	-0,27	0,039	0,84
10	-0,33	0,054	1,03

Table 5.2- Wing and Horizontal Tail tables of coefficient (angles in* deg*)

5.3 Complete aircraft

The fuselage is added to the SET to be analysed. The data collected later is a valuable contribution to the comparative analysis that will follow in the next paragraph.

AoA	CL	AoA	CL/CD
0	0,09	0	6,06
2	0,28	2	15,85
4	0,47	4	19,83
6	0,65	6	20,07
8	0,84	8	18,83
10	1,03	10	17,20

AoA	CMy	CDtot	CL
0	-0,01	0,010	0,09
2	-0,06	0,013	0,28
4	-0,11	0,019	0,47
6	-0,16	0,027	0,65
8	-0,21	0,039	0,84
10	-0,26	0,054	1,03

Table 5.3- Complete Aircraft tables of coefficient (angles in* deg*)

5.4 Aircraft component comparison curves

This section reports one of the main purposes of this thesis, show the contribution of the fuselage, and of the aircraft components to the aerodynamic coefficients.

The comparison curves of the aircraft, with the contribution of the fuselage, are shown below.

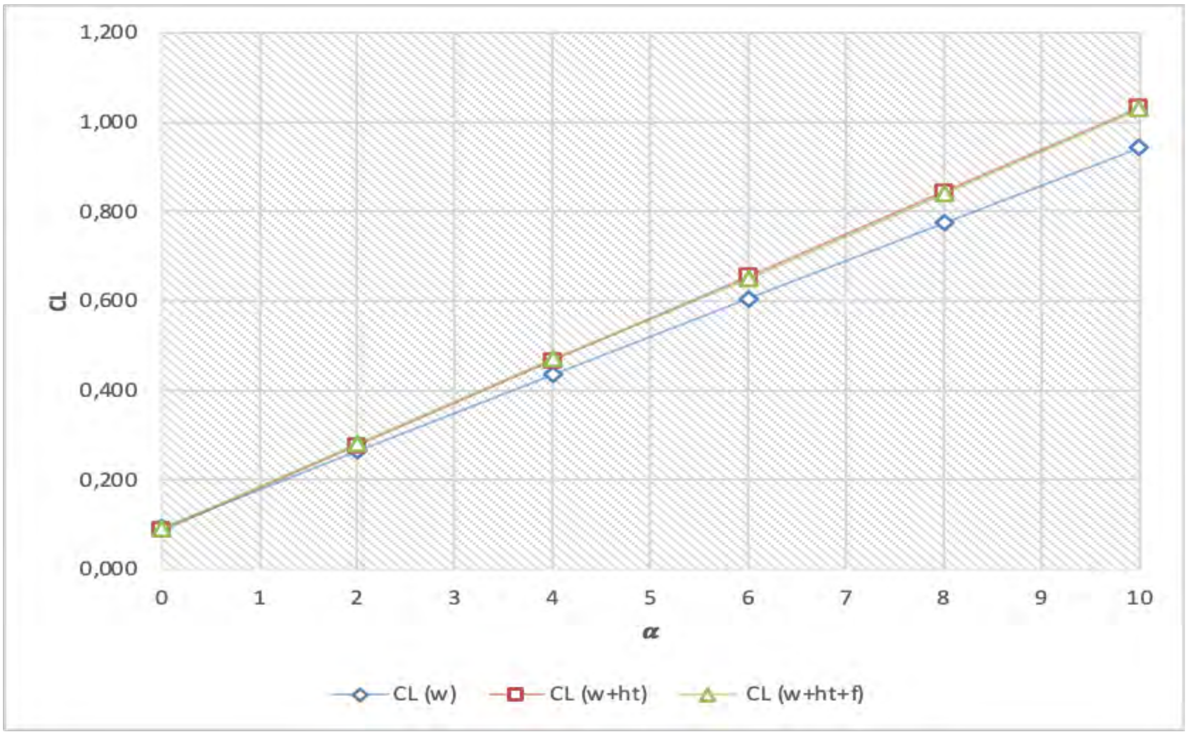

Figure 5.2 CL-α all components comparison plot (angles in deg)

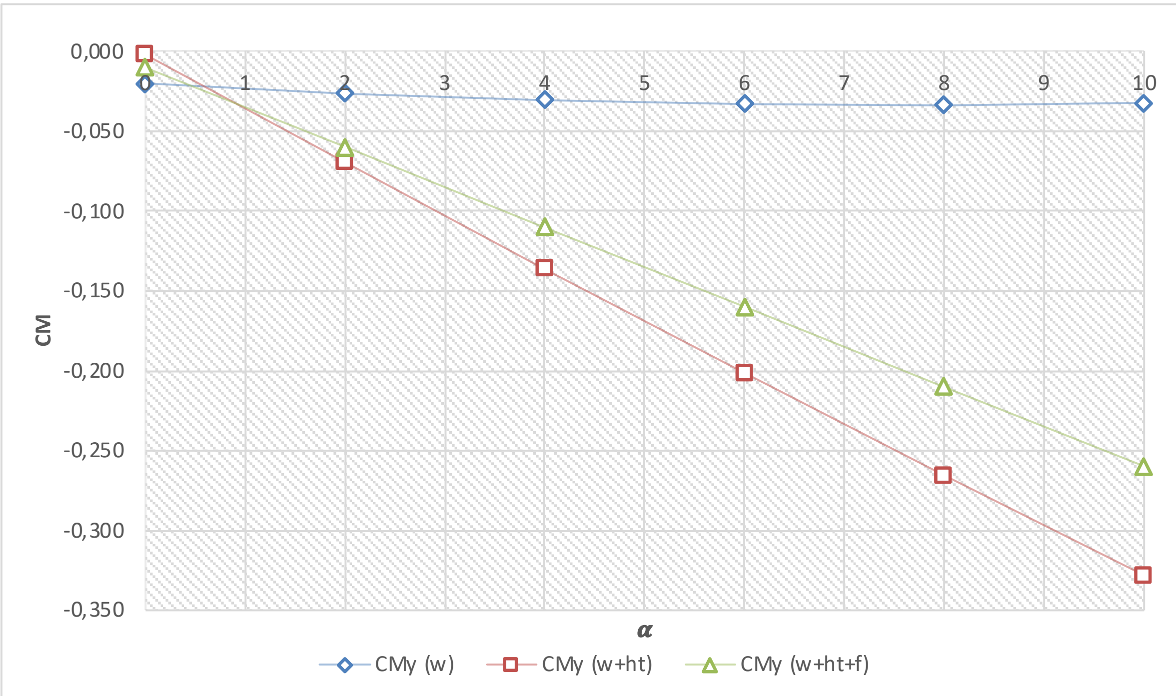

Figure 5.3 CM-α all components comparison plot (angles in deg)

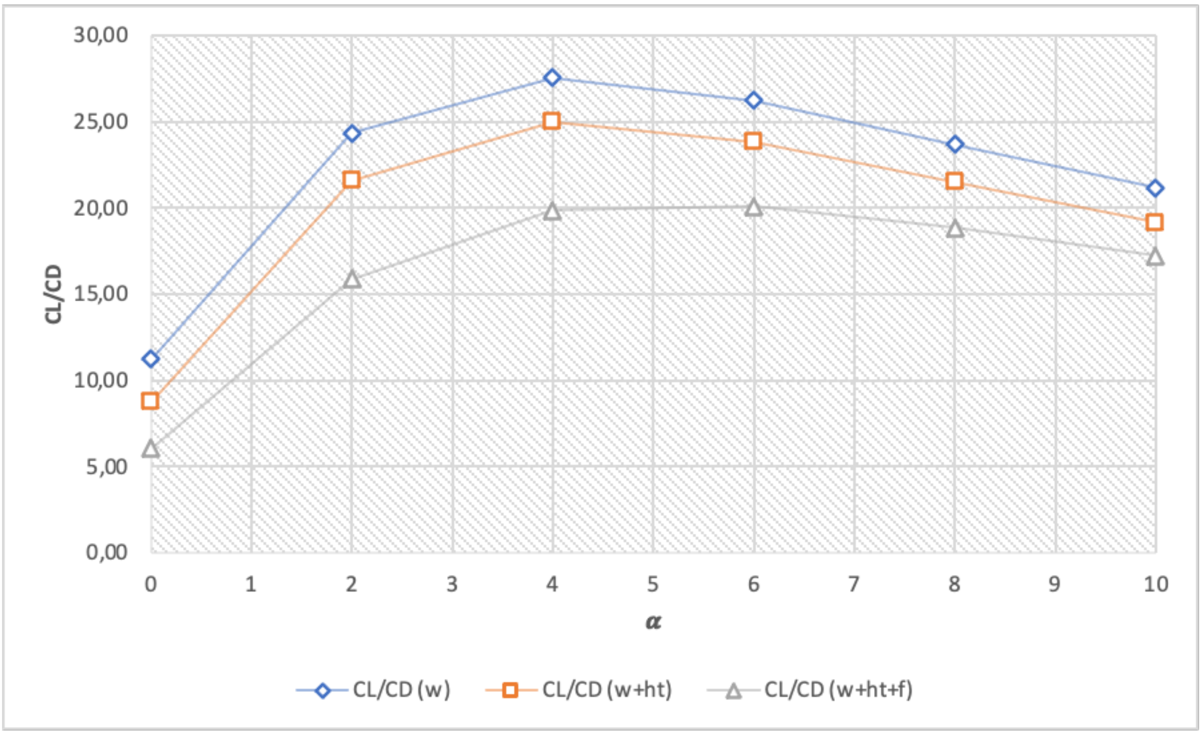

Figure 5.4 CL/CD-α components comparison plot (angles in deg)

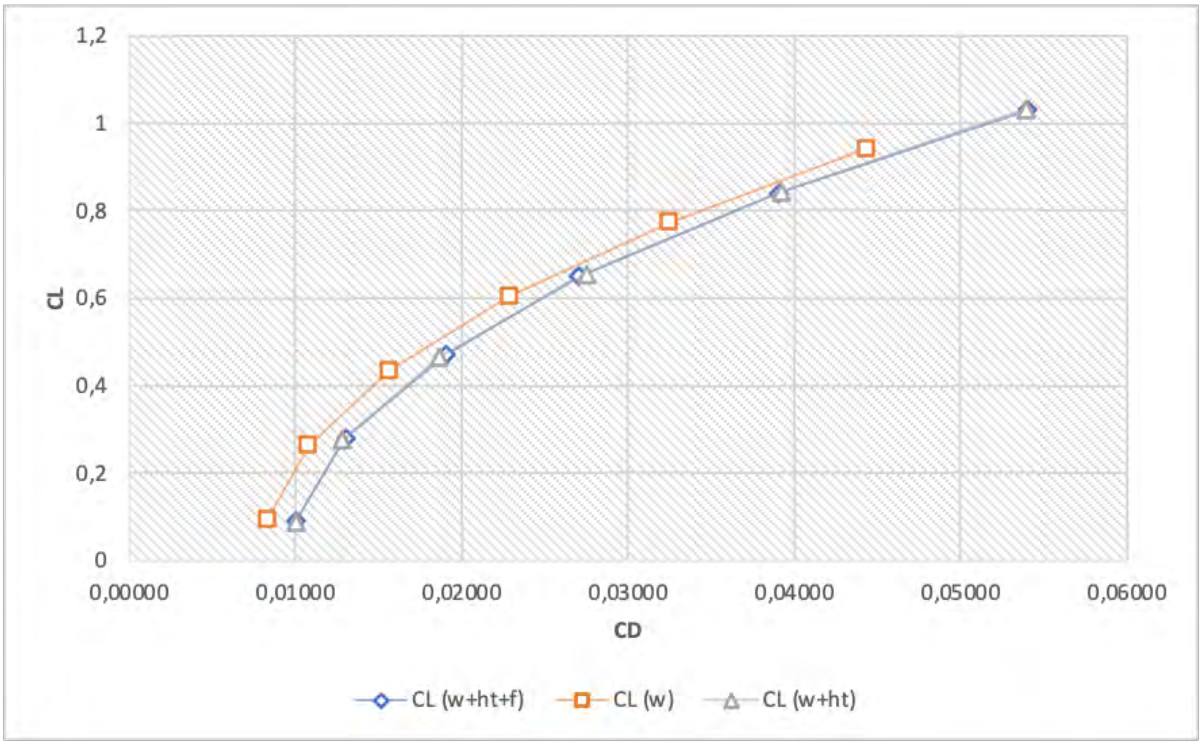

Figure 5.5 CL-CD all components comparison plot

What is immediately obvious is that adding Horizontal Tail and fuselage, the CL-α curve increases the slope (because we added a load-bearing surface, but the reference area to normalize CL remains the wing planform area S). Those in question are all untrimmed curves. The aerodynamic solver does not see the effect of the fuselage on the lift of the aircraft (which is generally very small compared to that of the wing anyway), but it does see it on the CM vs. alpha curve, i.e., the stability of the aircraft. Instead, the addition of the fuselage causes the CL/CD efficiency curve to translate downward, this is obviously because it increases the induced drag, and thus the CDtot. The curves shown were processed from an aerodynamic analysis with flaps deflected at 0°.

It is also possible to calculate the position of the neutral point.

The extended expression is:

$$\overline{XN} \equiv \frac{XN}{\bar{c}} = \frac{\bar{X}_{ac,WB} + \eta_H \frac{C_{L_{\alpha,H}}}{C_{L_{\alpha,WB}}} \frac{S_H \ \bar{X}_{ac,WB}\left[1-(\frac{d\epsilon}{d\alpha})_H\right]}{S}}{1+\eta_H \frac{C_{L_{\alpha,H}}}{C_{L_{\alpha,WB}}} \frac{S_H \left[1-(\frac{d\epsilon}{d\alpha})_H\right]}{S}}$$

From the concept of neutral point, we can define static stability margin:

$$SM = \overline{XG} - \overline{XN}$$

The static stability margin is usually a design requirement, with typical values of ≈ 0.10 ÷ 0.20. We can then make a further approximation assuming that $\overline{v_H}$ is independent from the position of the CG, and equating to zero the previous equation, we get the simplified expression of the neutral point:

$$\overline{XN} \approx \bar{X}_{ac,WB} + \eta_H \frac{C_{L_{\alpha,H}}}{C_{L_{\alpha,WB}}} \overline{v_H} \left[1 - (\frac{d\epsilon}{d\alpha})_H\right]$$

with

$$\overline{v_H} = \frac{S_H}{S}\frac{l_H}{\bar{c}} = \frac{S_H}{S}(\bar{X}_{ac,H} - \overline{XG})$$

We can easily prove further, that:

$$C_{M\alpha} = C_{L\alpha}(\overline{XG} - \overline{XN}) = C_{L\alpha}\, SM$$

We calculate the useful derivatives using the data from the previous tables for the three configurations, exploiting the Excel SLOPE function, for $C_{M\alpha}$ and $C_{L\alpha}$. We then run the ratio for the three cases considered. In the last row was naturally added to the contribution of the derivative, also the position of XG, placed at 25% of the aerodynamic chord.

	W	(W+HT)	(W+HT+F)
dCL_dα (1/deg)	0,085	0,094	0,094
dCM_dα (1/deg)	-0,001	-0,033	-0,025
- dCM_dα/dCL_dα	0,01	0,35	0,27
Aerodinamic center	0,26	0,60	0,52

Table 5.4- Table of the neutral point (angles in* deg, derivatives in 1/deg*)

In the third row are present the values of the static margin in the three cases, always assuming XG at 25%.

The next section will present a summary representation of a further analysis performed, the curves obtained from deflecting the flaps at 15° and 30°.

5.5 Flap deflection effects on curves

The software allows to perform analysis with the deflected moving surfaces (flaps), at different angles. A section of the VSPAERO panel is used.

Figure 5.6 FLAP panel

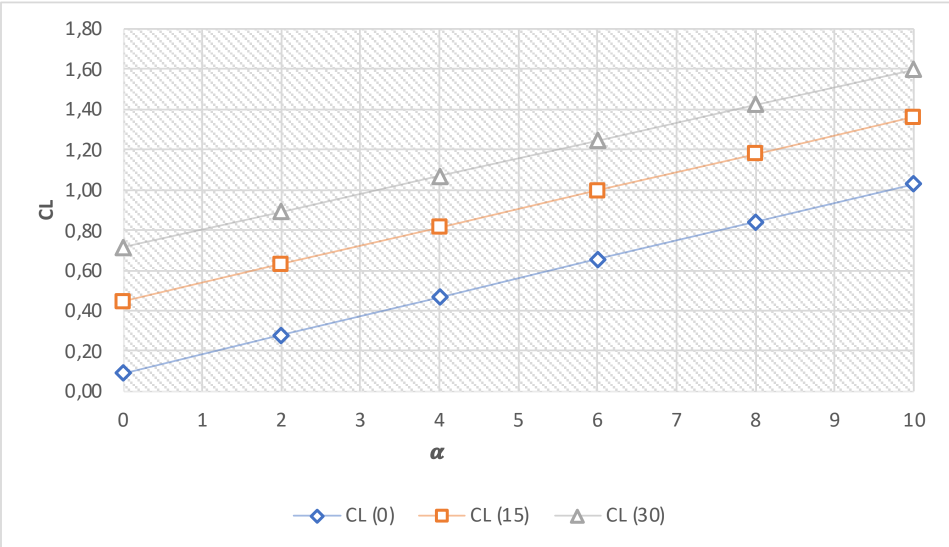

Figure 5.7 CL-α FLAP deflections effects comparison plot (angles in deg)

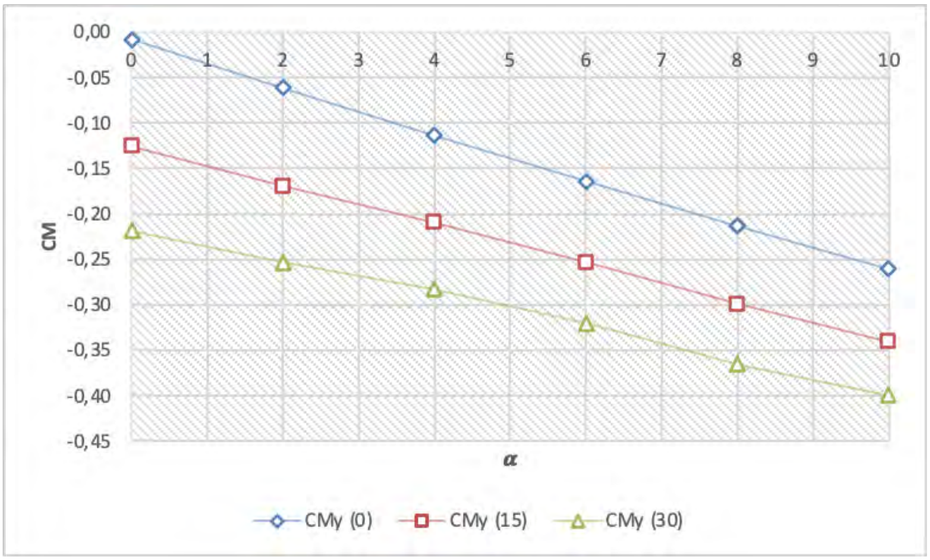

Figure 5.8 CM-α FLAP deflections effects comparison plot (angles in deg)

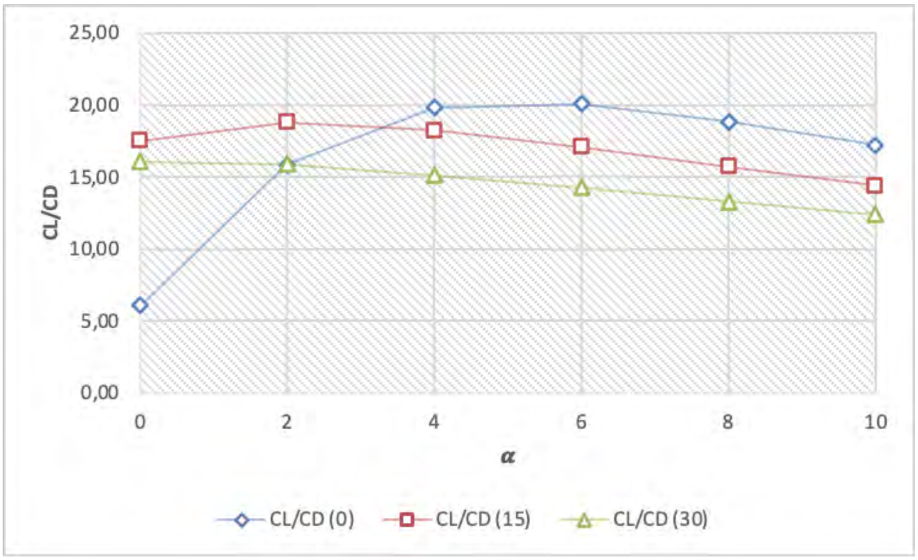

Figure 5.9 CL/CD-α FLAP deflections effects comparison plot (angles in deg)

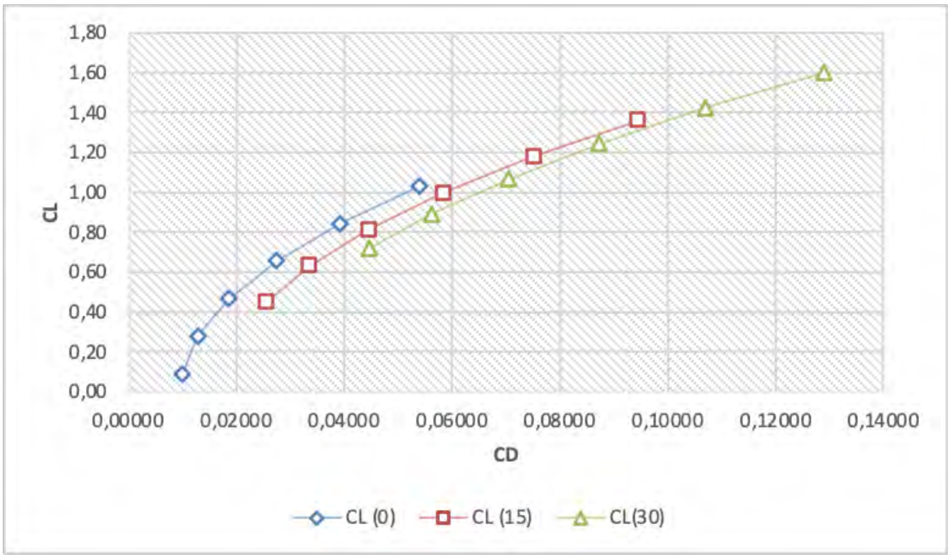

Figure 5.10 CL-CD FLAP deflections effects comparison plot

Also, those of the flaps, are not trimmed curves, which substantially move CL upwards, CM downwards, CD to the right. The aerodynamic efficiency worsens with the deflection due to increased aerodynamic drag, but VSPAERO sees well only the induced one, not the parasitic one.

5.6 Load distribution example

Logging into the OpenVSP folder and opening the file with the '.lod' extension, you can find useful data to plot the load distribution for various angles of attack.

The analysis was done for angle of attack of 4° and the three different flap deflections, so again comparison curves in *Figure 5.11* were produced.

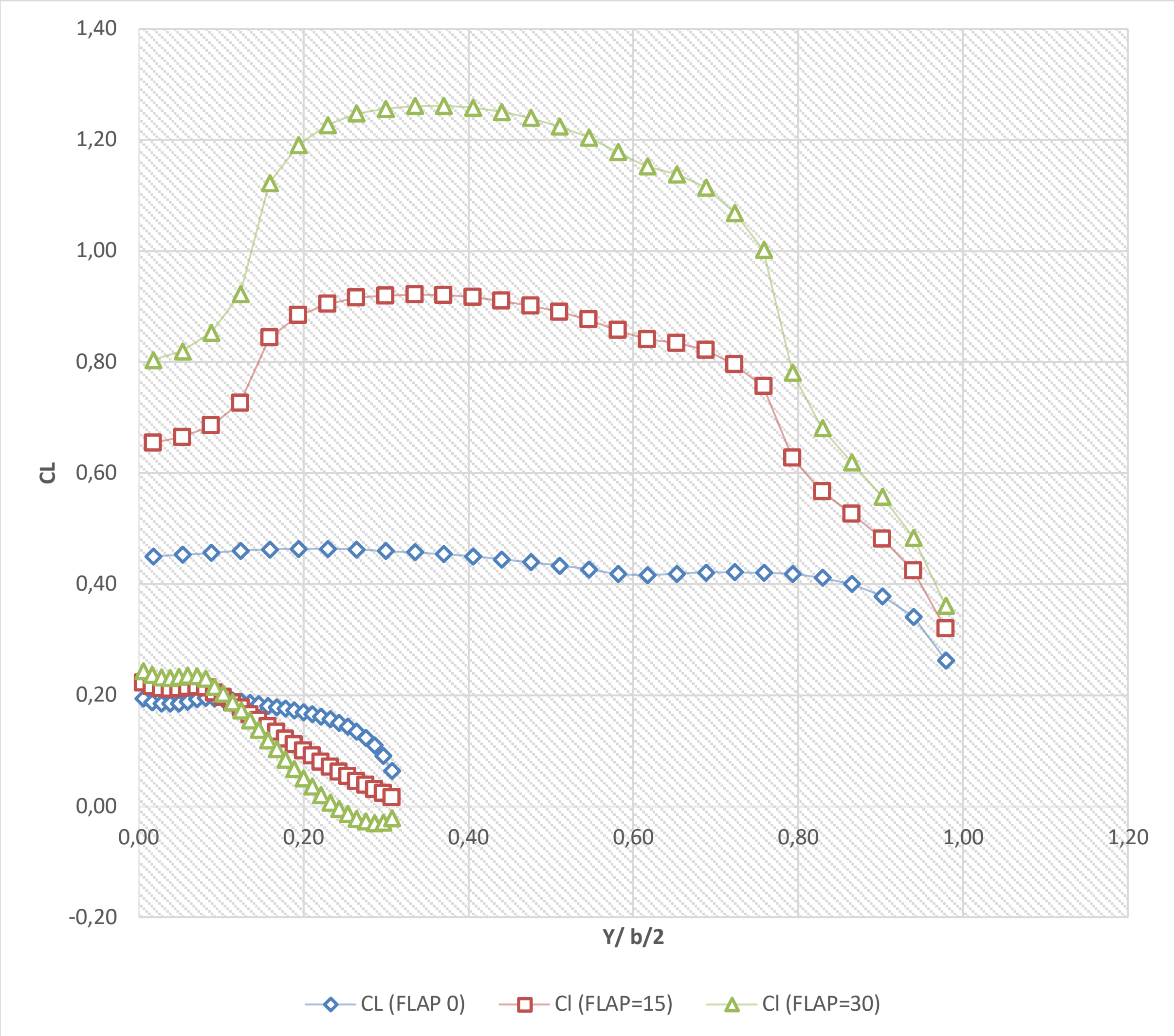

Figure 5.11 FLAP deflections effects on LOAD- comparison plot

The graph in Figure *5.11* is obtained from *Table 5.5*. Opening the '.lod' file, we chose to diagram the Yavg, scaled on the wing half-opening, with the CL.

	WING		
Yavg/0,750	CL (FLAP 0)	Cl (FLAP=15)	Cl (FLAP=30)
0,02	0,45	0,65	0,80
0,05	0,45	0,66	0,82
0,09	0,46	0,69	0,85
0,12	0,46	0,73	0,92
0,16	0,46	0,84	1,12
0,19	0,46	0,88	1,19
0,23	0,46	0,90	1,23
0,26	0,46	0,92	1,25
0,30	0,46	0,92	1,26
0,33	0,46	0,92	1,26
0,37	0,45	0,92	1,26
0,40	0,45	0,92	1,26
0,44	0,45	0,91	1,25
0,48	0,44	0,90	1,24
0,51	0,43	0,89	1,22
0,55	0,43	0,88	1,20
0,58	0,42	0,86	1,18
0,62	0,42	0,84	1,15
0,65	0,42	0,83	1,14
0,69	0,42	0,82	1,11
0,72	0,42	0,80	1,07
0,76	0,42	0,76	1,00
0,79	0,42	0,63	0,78
0,83	0,41	0,57	0,68
0,87	0,40	0,53	0,62
0,90	0,38	0,48	0,56
0,94	0,34	0,42	0,48
0,98	0,26	0,32	0,36
	Horizontal Tail		
0,01	0,19	0,22	0,24
0,02	0,19	0,22	0,24
0,03	0,19	0,21	0,23
0,04	0,19	0,21	0,23
0,05	0,19	0,21	0,23
0,06	0,19	0,22	0,24
0,07	0,19	0,22	0,24
0,08	0,20	0,21	0,23
0,09	0,19	0,20	0,22
0,10	0,19	0,20	0,20
0,11	0,19	0,19	0,19
0,12	0,19	0,18	0,17
0,13	0,19	0,17	0,15
0,15	0,18	0,16	0,14
0,16	0,18	0,14	0,12
0,17	0,18	0,13	0,10
0,18	0,18	0,12	0,08
0,19	0,17	0,11	0,07
0,20	0,17	0,10	0,05
0,21	0,17	0,09	0,04
0,22	0,16	0,08	0,02
0,23	0,16	0,07	0,01
0,24	0,15	0,06	0,00
0,25	0,14	0,05	-0,01
0,26	0,14	0,05	-0,02
0,27	0,12	0,04	-0,03
0,29	0,11	0,03	-0,03
0,30	0,09	0,02	-0,03
0,31	0,06	0,02	-0,02

Table 5.5- FLAP deflections effects on LOAD- comparison table

On the graph in Figure *5.10,* relative to the *Table 5.5*, there are two pairs of curves, one related to the wing, and the other to the Horizontal Tail.

The presence of the deflected flaps causes a 'hump' to be generated on the graph, which is more pronounced for higher deflections.

5.7 Stability and control consideration

DATA		
# Name	Value	Units
Sref_	0,25	Lunit^2
Cref_	0,171	Lunit
Bref_	1,5	Lunit
Xcg_	0,418	Lunit
Ycg_	0	Lunit
Zcg_	0,107	Lunit
Mach_	0	no_unit
AoA_	0	deg
Beta_	0	deg
Rho_	1,225	Munit/Lunit^3
Vinf_	35	Lunit/Tunit
Roll__Rate	0	rad/Tunit
Pitch_Rate	0	rad/Tunit
Yaw___Rate	0	rad/Tunit

Table 5.6- Background data for control and stability analysis table (SI units)

In the table above, we observe the starting values set to start the control and stability analysis. This analysis aims to apply variations of a delta equal to 1 deg to the angles, starting from the data initially entered. These data are collected in *Table 5.6*, along with the dynamic, control and stability derivatives.

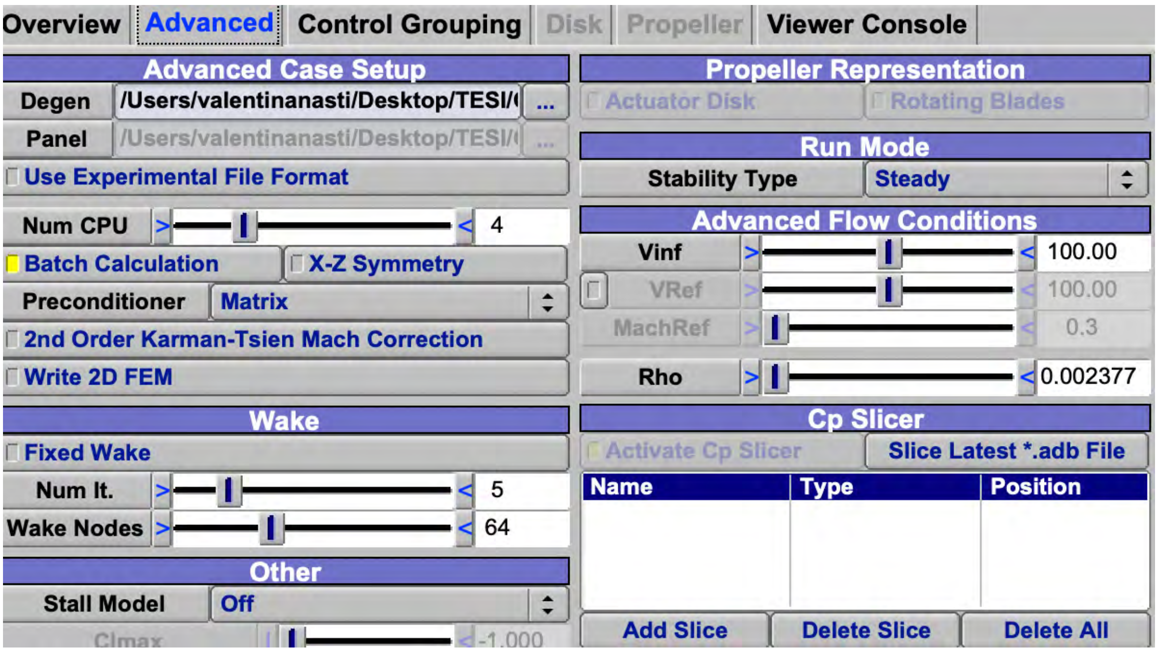

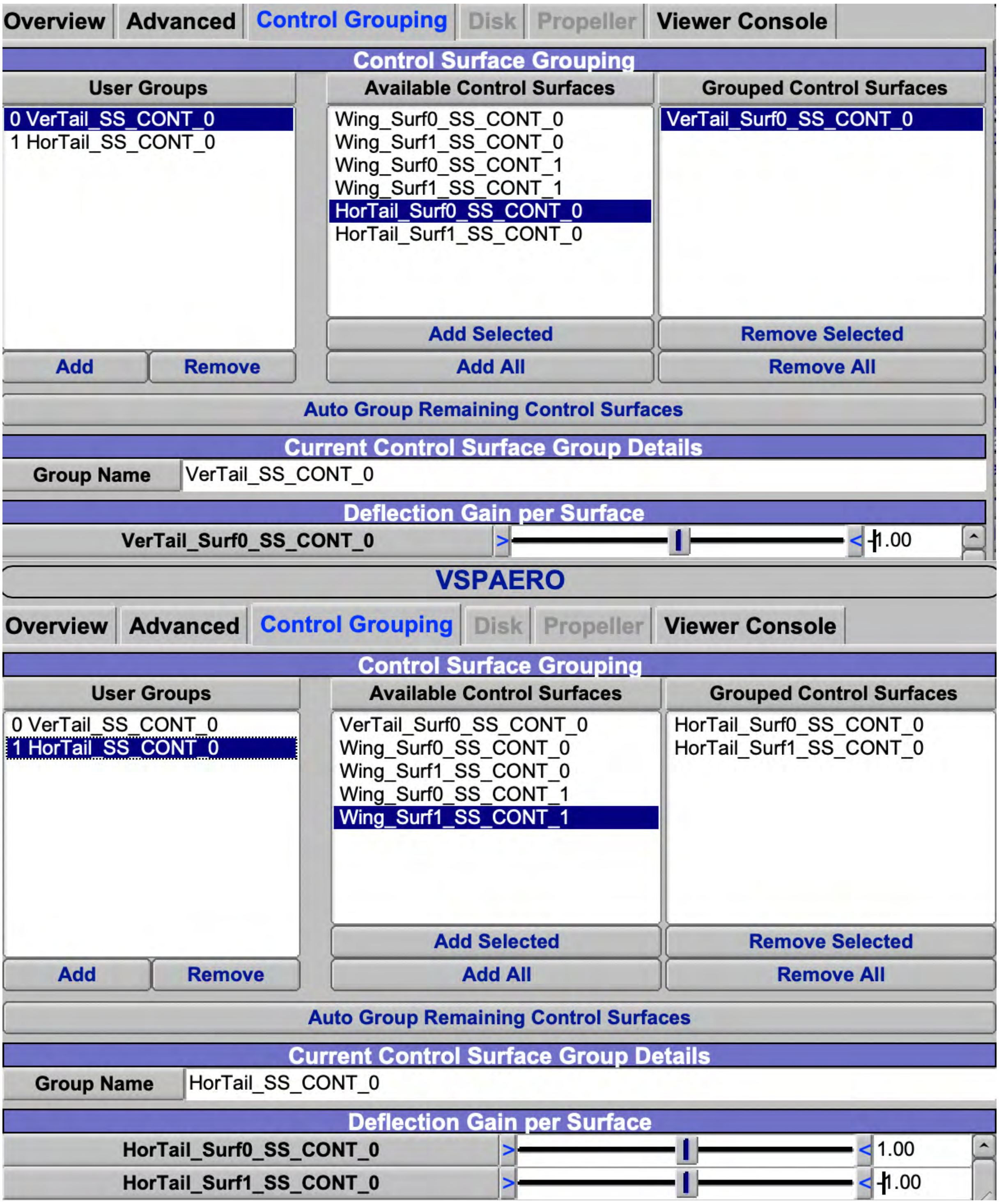

Figure 5.12 VSPAERO control panel for stability calculation

The panels shown above, allow you to select control surfaces and activate deflection. We are going to click on the 'Auto Group Remaining Control Surfaces' button. Ignoring the flaps, thus the wings, already dealt earlier, we are going to enter unit deflection in the panel for both the vertical and horizontal planes. Sometimes you have to change the gain sign of the movable surface to ensure proper deflection. Because VSPAERO's setting has opposite directions of rotation in the moving surfaces of the horizontal tail, we enter -1 for one of the elevators, such that a positive rotation corresponds to a downward deflection of both elevators. We enter it negative for the deflection of vertical tail.

Case	Delta	Units	CFx	CFy	CFz	CMx	CMy	CMz	CL	CD	CS	CMl	CMm	CMn
#														
Base_Aero	0	n/a	0,000	0,000	0,090	0,000	-0,010	0,000	0,090	0,000	0,000	0,000	-0,010	0,000
Alpha	1	deg	-0,002	0,000	0,184	0,000	-0,037	0,000	0,184	0,001	0,000	0,000	-0,037	0,000
Beta	1	deg	0,000	-0,004	0,090	0,000	-0,010	0,000	0,090	0,000	-0,004	0,000	-0,010	0,000
Roll__Rate	1	rad/Tunit	0,000	0,001	0,090	0,012	-0,010	0,000	0,090	0,000	0,001	-0,012	-0,010	0,000
Pitch_Rate	1	rad/Tunit	0,000	0,000	0,118	0,000	-0,058	0,000	0,118	0,000	0,000	0,000	-0,058	0,000
Yaw___Rate	1	rad/Tunit	0,000	0,005	0,090	-0,001	-0,010	0,001	0,090	0,000	0,005	0,001	-0,010	-0,001
Mach	0,1	no_unit	0,000	0,000	0,090	0,000	-0,010	0,000	0,090	0,000	0,000	0,000	-0,010	0,000
VerTail_SS_CC	1	deg	0,000	0,003	0,090	0,000	-0,010	0,001	0,090	0,000	0,003	0,000	-0,010	-0,001
HorTail_SS_CC	1	deg	0,000	0,000	0,097	0,000	-0,034	0,000	0,097	0,000	0,000	0,000	-0,034	0,000

***Table 5.7- Table of angle increments (angles in* rad)**

We are going to highlight the derivatives:

- $\boldsymbol{CL_\alpha}$, $\boldsymbol{CMy_\alpha}$, $\boldsymbol{CMx_\beta}$, $\boldsymbol{CMz_\beta}$,(stability derivatives).
- CMy_q, CMz_r, CMx_p (dynamic derivatives).
- $CL\delta_e$, $CMy\delta_e$, $CMx\delta_r$ $CMz\delta_r$ (control derivatives).

The *Table 5.7* on the following page collects and highlights them in relation to the other parameter after having converted them into 1/deg. The following are all evaluated in a constructive reference system (x to the stern, z to the top, y to the right) with origin in the chosen pole (25% m.a.c.).

#	Base	Derivative:								
#	Aero	wrt	wrt	wrt	wrt	wrt	wrt	wrt	wrt	wrt
Coef	Total	Alpha	Beta	p	q	r	Mach	U	VerTail	HorTail
#	-	per	per	per	per	per	per	per	per	per
#	-	deg	deg	deg	deg	deg	M	u	deg	deg
#										
CFx	0,00015	-0,00234	-0,00006	-0,00028	-0,00136	-0,00004	0,00002	0,00000	0,00001	0,00003
CFy	-0,00002	0,00000	-0,00439	0,00090	0,00001	0,00380	0,00000	0,00000	0,00279	0,00000
CFz	0,08992	0,09446	-0,00005	-0,00002	0,19815	0,00003	0,00328	0,00000	0,00000	0,00682
CMx	-0,00001	0,00000	0,00020	0,00938	0,00001	-0,00042	0,00000	0,00000	-0,00004	0,00000
CMy	-0,01018	-0,02669	0,00014	0,00012	-0,34115	0,00000	0,00040	0,00000	0,00001	-0,02343
CMz	-0,00001	0,00000	-0,00036	0,00039	0,00001	0,00120	0,00000	0,00000	0,00106	0,00000
CL	0,08992	0,09447	-0,00005	-0,00002	0,19815	0,00003	0,00328	0,00000	0,00000	0,00682
CD	0,00015	0,00088	0,00002	-0,00028	-0,00136	-0,00004	0,00002	0,00000	0,00001	0,00003
CS	-0,00002	0,00000	-0,00439	0,00090	0,00001	0,00380	0,00000	0,00000	0,00279	0,00000
CMl	0,00001	0,00000	-0,00020	-0,00938	-0,00001	0,00042	0,00000	0,00000	0,00004	0,00000
CMm	-0,01018	-0,02669	0,00014	0,00012	-0,34115	0,00000	0,00040	0,00000	0,00001	-0,02343
CMn	0,00001	0,00000	0,00036	-0,00039	-0,00001	-0,00120	0,00000	0,00000	-0,00106	0,00000

Stability derivatives

Dynamic derivatives

Control derivatives

Table 5.8- Table of derivatives (**derivatives in 1/deg*****)***

6. Conclusions

At the end of this thesis, it can be concluded that VSPAERO satisfies excellent design.

In the preliminary design of aircraft, VSPAERO can provide a rough idea of the aerodynamics of the design, without having to perform extensive CFD simulations or wind tunnel tests. This can save a significant amount of time in the design process.

Obviously, there are several defects: The flow conditions are simplified and therefore VSPAERO will not provide exact results, as its main purpose is to be designed to give quick results. In addition, the model used in the simulations must be carefully refined to obtain relevant results as a result. It certainly has limits for more complex models, however it is a good solution for simple projects that require a first numerical analysis to be compared with real tests in the wind tunnel.

Bibliography

[1] Ambrosino, De Martino, “Aerodynamic analysis and surrogate modelling of distributed propulsion on commuter and regional aircraft through VLM and CFD methods”, 2019.

[2] Floris Mariën, “Software Testing: VSPAERO”,2021.

[3] Liu, Chao, “Wake Vortex Encounter Analysis with Different Wake Vortex Models Using Vortex-Lattice Method”,2007.

[4] Robert A. McDonald, State University of San Luis Obispo, “Advanced Modeling in OpenVSP”,2016.

[5] http://openvsp.org

[6] http://airfoiltools.com